3.1 Linear optics

R. Güther

The propagation of light and its interaction with matter is completely described by *Maxwell's equations* (1.1.4)–(1.1.7) and the material equations (1.1.8) and (1.1.9), see Chap. 1.1.

In this chapter the propagation of light in dielectric homogeneous and nonmagnetic media is discussed. Furthermore, monochromatic waves are assumed and linear interaction. The implications thereof for the medium are:

- *Relative permittivity:* ε_r ($\varepsilon(\boldsymbol{E},\boldsymbol{H})$ in (1.1.8)) is a complex tensor, which in most cases depends on the frequency only, but in special cases also on the spatial coordinate.
- *Relative permeability:* $\mu_\mathrm{r} = 1$ ($\mu(\boldsymbol{E},\boldsymbol{H})$ in (1.1.9)).
- *Electrical charge density:* $\rho = 0$.
- *Current density:* $j = 0$.

3.1.1 Wave equations

Maxwell's equations together with the material equations and the above assumptions result in the time-dependent wave equation for the electric field

$$\Delta\,\boldsymbol{E}(\boldsymbol{r},t) - \frac{\varepsilon_\mathrm{r}}{c_0^2}\frac{\partial^2}{\partial t^2}\boldsymbol{E}(\boldsymbol{r},t) = 0 \tag{3.1.1}$$

with

$c_0 = 2.99792458 \times 10^8$ m/s: vacuum velocity of light,

$$\Delta = \frac{\partial^2}{\partial\, x^2} + \frac{\partial^2}{\partial\, y^2} + \frac{\partial^2}{\partial\, z^2} \;:\quad \text{delta operator.}$$

An identical equation holds for the magnetic field $\boldsymbol{H}(\boldsymbol{r},t)$.

For the following discussion we assume monochromatic fields, so that

$$\boldsymbol{E}(\boldsymbol{r},t) = \boldsymbol{E}(\boldsymbol{r})\,\mathrm{e}^{\mathrm{i}\,\omega\,t} \tag{3.1.2}$$

with

ω: angular temporal frequency.

The magnetic field is related to $\boldsymbol{E}$ by the corresponding Maxwell equation (1.1.7)

$$\mathrm{curl}\,\boldsymbol{E}(\boldsymbol{r}) = -\mathrm{i}\,\omega\,\mu_0\boldsymbol{H}(\boldsymbol{r})\,. \tag{3.1.3}$$

Together with the ansatz (3.1.2), for isotropic media (ε_r is a complex scalar) (3.1.1) results in

$$\Delta\,\boldsymbol{E}(\boldsymbol{r}) + k_0^2\,\hat{n}^2\,\boldsymbol{E}(\boldsymbol{r}) = 0 \quad (\textit{wave equation}) \tag{3.1.4}$$

with

$k_0 = 2\pi/\lambda_0$: *wave number*,
λ_0 : wavelength in vacuum,
$\hat{n}$: complex refractive index, see (1.1.20).

For isotropic media and fields with uniform polarization the vector property of the field can be neglected. This results in

$$\Delta E(\boldsymbol{r}) + k_0^2 \hat{n}^2 E(\boldsymbol{r}) = 0 \quad (\textit{Helmholtz equation}). \tag{3.1.5}$$

In most cases the field can be approximated by a quasiplane wave, propagating in z-direction

$$\boldsymbol{E} = \boldsymbol{E}_0(\boldsymbol{r})\, \mathrm{e}^{\mathrm{i}(\omega t - k_0 \hat{n} z)} \,. \tag{3.1.6}$$

Remark: There are different *conventions* for writing the complex wave (3.1.6):

1. Electrical engineering and most books on quantum electronics:

$$\boldsymbol{E} \propto \exp(\mathrm{i}\,\omega t - \mathrm{i}\, k_0 \hat{n} z) \,,$$

for example [96Yar, 86Sie, 66Kog2, 84Hau, 91Sal, 98Sve, 96Die] and this chapter, Chap. 3.1.

2. Physical optics:

$$\boldsymbol{E} \propto \exp(\mathrm{i}\, k_0 \hat{n} z - \mathrm{i}\,\omega t) \,,$$

for example [99Bor, 92Lan, 75Jac, 05Hod, 98Hec, 70Col].

[94Fel] discusses both cases.
Consequences of the convention: shape of results on phases of wave propagation, diffraction, interferences, Jones matrix, Collins integral, Gaussian beam propagation, absorption, and gain.

With

$$\left| \frac{\partial \boldsymbol{E}_0}{\partial z} \right| \ll |k_0 \hat{n}\, \boldsymbol{E}_0|$$

(3.1.4) can be reduced to

$$\Delta_\mathrm{t} \boldsymbol{E}_0 + 2\,\mathrm{i}\, k_0 \hat{n} \frac{\partial\, \boldsymbol{E}_0}{\partial\, z} = 0 \quad (\textit{Slowly Varying Envelope (SVE) equation}) \,, \tag{3.1.7}$$

with

$$\Delta_\mathrm{t} = \frac{\partial^2}{\partial\, x^2} + \frac{\partial^2}{\partial\, y^2} \;: \quad \text{transverse delta operator (rectangular symmetry)},$$

see Chap. 1.1, (1.1.24a). *Other names for SVE* are: paraxial wave equation [86Sie], paraxial Helmholtz equation [96Ped, 78Gra].

The analogue approximation with respect to time t instead of the spatial coordinate z is used in ultrashort laser pulse physics [96Die, 86Sie].

3.1.2 Polarization

Restriction of (3.1.2) to a plane wave along the z-axis, see Fig. 3.1.1, results in

$$\begin{bmatrix} E_x \\ E_y \end{bmatrix} = \begin{bmatrix} E_{0x}\,\cos\left(\omega\,t - kz + \delta_x\right) \\ E_{0y}\,\cos\left(\omega\,t - kz + \delta_y\right) \end{bmatrix} \Rightarrow$$

$$\begin{bmatrix} E_{0x}\,\exp(\mathrm{i}\,\delta_x) \\ E_{0y}\,\exp(\mathrm{i}\,\delta_y) \end{bmatrix} \exp\left[\mathrm{i}\,(\omega\,t - kz)\right] \equiv E_0\,\boldsymbol{J}\exp\left[\mathrm{i}\,(\omega\,t - kz)\right]\ . \tag{3.1.8}$$

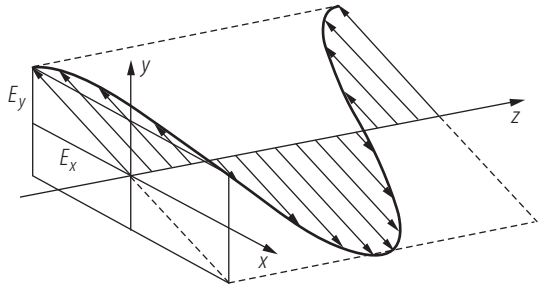

Fig. 3.1.1. Electric field of a linear polarized wave with propagation along the z-axis.

Definitions:

$E_0 = \sqrt{E_{0x}^2 + E_{0y}^2}$,

$\boldsymbol{J} = \dfrac{1}{E_0}\begin{bmatrix} E_{0x}\,\exp(\mathrm{i}\,\delta_x) \\ E_{0y}\,\exp(\mathrm{i}\,\delta_y) \end{bmatrix}$: (*normalized*) *Jones vector* ,

δ_x and δ_y : phase angles ,

$\Rightarrow$: transition to the complex representation ,

$\varepsilon_0 n c_0\,E_0^2\boldsymbol{J}\boldsymbol{J}^*/2$: light intensity [W/m^2] .

Different *conventions* for *right*-hand polarization:

1. Looking against the direction of light propagation the light vector moves clockwise in the x-y-plane of Fig. 3.1.1 ([99Bor, 91Sal, 96Ped, 98Hec, 88Kle, 87Nau]).
2. The clockwise case occurs looking with the propagation direction (right-hand screw, elementary particle physics) ([84Yar, 88Yeh, 05Hod] and *in this chapter*).

Remark: $\boldsymbol{J}$ without normalization is also called Jones vector in [84Yar, 88Yeh, 90Roe, 77Azz, 86Sol], [95Bas, Vol. II, Chap. 27].

Jones Calculus [41Jon, 97Hua, 88Yeh, 90Roe, 75Ger]:

$$\mathsf{J}_2 = \mathsf{M}\,\mathsf{J}_1 \tag{3.1.9}$$

with

J_1 : Jones matrix for the initial polarization state,
M : Jones matrix describing an optical element or system,
J_2 : Jones matrix of the polarization state after light has passed the element or system.

In Table 3.1.1 the characterization of the polarization states of light with the *Jones vector* is given, in Table 3.1.2 the characterization of optical elements with the *Jones matrix*.

Table 3.1.1. Characterization of the polarization states of light with the *Jones vector*.

Jones vector $\boldsymbol{J}$	$\begin{bmatrix}\cos\psi\\ \sin\psi\end{bmatrix}$	$\frac{1}{\sqrt{2}}\begin{bmatrix}1\\ \mathrm{i}\end{bmatrix}$	$\frac{1}{\sqrt{2}}\begin{bmatrix}\mathrm{i}\\ 1\end{bmatrix}$	$\begin{bmatrix}a\cdot\mathrm{i}\\ b\end{bmatrix}$ and $a^2+b^2=1$
State of polarization	Linear polarization	Left circular polarization	Right circular polarization	Right elliptical polarization
Projection of the vector $\boldsymbol{E}$ onto the x-y-plane viewed along the propagation direction z	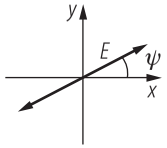	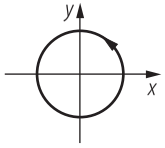	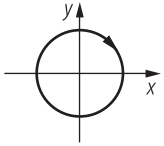	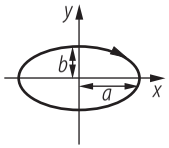

Table 3.1.2. Characterization of optical elements with the *Jones matrix*.

Opt. Element	Polarizer along the x-direction	Polarizer along the y-direction	Quarter-wave plate	Half-wave plate	Brewster-angle-tilted plate: index n	Faraday rotator (angle β)	Coordinate rotation by an angle α: $\mathsf{M}(\alpha)$
Jones Matrix	$\begin{bmatrix}1&0\\0&0\end{bmatrix}$	$\begin{bmatrix}0&0\\0&1\end{bmatrix}$	$\begin{bmatrix}1&0\\0&\pm\mathrm{i}\end{bmatrix}$	$\begin{bmatrix}1&0\\0&-1\end{bmatrix}$	$\begin{bmatrix}\left[\frac{2n}{n^2+1}\right]^2&0\\0&1\end{bmatrix}$	$\begin{bmatrix}\cos\beta&-\sin\beta\\ \sin\beta&\cos\beta\end{bmatrix}$	$\begin{bmatrix}\cos\alpha&\sin\alpha\\ -\sin\alpha&\cos\alpha\end{bmatrix}$ Rotated element: $\mathsf{M}(\alpha)\,\mathsf{M}\,\mathsf{M}(-\alpha)$

Example 3.1.1.

$$\mathsf{M} = \mathsf{M}_3 \cdot \mathsf{M}_2 \cdot \mathsf{M}_1 \ , \tag{3.1.10}$$

M: Jones matrix of the system which consists of elements with the matrices M_1, M_2, M_3. Light passes first the element with M_1 and last the element with M_3.

Example 3.1.2. $\boldsymbol{J}_1 = \frac{1}{\sqrt{2}} \begin{bmatrix} 1 \\ 1 \end{bmatrix}$ (linear 45°-polarization), $\mathsf{M} = \begin{bmatrix} 1 & 0 \\ 0 & \pm\mathrm{i} \end{bmatrix}$ ($\left\{ \begin{matrix} \text{right} \\ \text{left} \end{matrix} \right\}$ quarter-wave plate), $\boldsymbol{J}_2 = \mathsf{M} \cdot \boldsymbol{J}_1 = \frac{1}{\sqrt{2}} \begin{bmatrix} 1 \\ \pm\mathrm{i} \end{bmatrix}$ ($\left\{ \begin{matrix} \text{right} \\ \text{left} \end{matrix} \right\}$ circular polarization).

Development: Any Jones vector can be developed into a superposition of two orthogonal Jones vectors:

$$\boldsymbol{J} = a_1 \boldsymbol{J}_1 + a_2 \boldsymbol{J}_2 \tag{3.1.11}$$

with $\boldsymbol{J}_1 \boldsymbol{J}_2^* = 0$.

Example 3.1.3. linearly polarized light = left polarized light + right polarized light .

Partially polarized light: If parts of both coefficients of the $\boldsymbol{E}$-vector are uncorrelated, there is a mixing of polarized and *non*polarized light. It is described by the four components of the *Stokes vector* $\{s_0, s_1, s_2, s_3\}$, using $\langle \dots \rangle$ to signify averaging by detection:

$$s_0 = \langle E_x^2 \rangle + \langle E_y^2 \rangle \quad \Rightarrow \quad E_{0x}^2 + E_{0y}^2 \ , \tag{3.1.12}$$

$$s_1 = \langle E_x^2 \rangle - \langle E_y^2 \rangle \quad \Rightarrow \quad E_{0x}^2 - E_{0y}^2 \ , \tag{3.1.13}$$

$$s_2 = 2 \langle E_x E_y \cos[\delta_y - \delta_x] \rangle \quad \Rightarrow \quad 2 E_{0x} E_{0y} \cos(\delta_y - \delta_x) \ , \tag{3.1.14}$$

$$s_3 = 2 \langle E_x E_y \sin[\delta_y - \delta_x] \rangle \quad \Rightarrow \quad 2 E_{0x} E_{0y} \sin(\delta_y - \delta_x) \tag{3.1.15}$$

with

$$s_0^2 > s_1^2 + s_2^2 + s_3^2 \quad \Rightarrow \quad s_0^2 = s_1^2 + s_2^2 + s_3^2 \ , \tag{3.1.16}$$

where $\Rightarrow$ means the transition from partially polarized light to completely polarized light, shown with the terms of Fig. 3.1.1.

Meaning of the s_i:
s_0: power flux,
$\sqrt{s_1^2 + s_2^2 + s_3^2}/s_0$: degree of polarization,
$\sqrt{s_1^2 + s_2^2}/s_0$: degree of linear polarization,
s_3/s_0: degree of circular polarization.

Mueller calculus ([75Ger, 77Azz, 90Roe, 95Bas]): extension of the *Jones calculus* for *partial-coherent light*, where the four dimensional Stokes vector replaces the Jones vector and the real 4×4 Mueller matrices the complex 2×2 Jones matrices. The Jones calculus is usually sufficient to describe coherent laser radiation.

Measurement of the polarization state:

- *Partially polarized light*: [87Nau], [76Jen, Chap. 27.6], [77Azz, Chap. 3], [61Ram, Sect. 14–25], [95Bas, Vol. 2, Chap. 22.15], [75Ger]. Result: Stokes vector.
- *Pure coherent light*: see [05Hod]. There are commercial systems for this task.

Eigenstates of polarized light are those two polarization states (Jones vectors) which reproduce themselves, multiplied with a complex factor (eigenvalue), if monochromatic light passes an optical element or system.

Calculation: see [97Hua, 77Azz], application: decoupling of the polarization mixing during round trips in resonators [74Jun].

3.1.3 Solutions of the wave equation in free space

Following (3.1.2), each of the wave solutions given in this section must be multiplied with the factor $e^{i\omega t}$ to obtain the propagating wave of (3.1.1).

3.1.3.1 Wave equation

The solutions of the wave equation (3.1.4) are vector fields.

3.1.3.1.1 Monochromatic plane wave

$$\boldsymbol{E} = \boldsymbol{E}_0 \exp\{-i\, k_0\, \hat{n}\, \boldsymbol{e}\boldsymbol{r} + i\,\varphi\}\ , \tag{3.1.17}$$

$$\boldsymbol{H} = \frac{\hat{n}}{c_0\mu_0}\,(\boldsymbol{e}\times\boldsymbol{E}_0)\exp\{-i\, k_0\, \hat{n}\, \boldsymbol{e}\boldsymbol{r} + i\,\varphi\} \tag{3.1.18}$$

with

$\boldsymbol{r}$: position vector,
$\boldsymbol{e}$: unit vector normal to the wave fronts,
$k_0 = 2\pi/\lambda_0$: wave number,
$\hat{n}$: complex refractive index,
φ : phase.

For the phase velocity and the wave group velocity see Sect. 3.1.5.3.

3.1.3.1.2 Cylindrical vector wave

$$\boldsymbol{E} = E_0\, \boldsymbol{e}_z\, H_0^{(2)}(k_0\rho)\ , \tag{3.1.19}$$

$$\boldsymbol{H} = i\frac{E_0}{c_0\mu_0}\left(\boldsymbol{e}_z \times \frac{\boldsymbol{\rho}}{\rho}\right) H_1^{(2)}(k_0\rho) \quad (\rho > \lambda) \tag{3.1.20}$$

for time-harmonic electric source current density on the z-axis of a cylindrical coordinate system with the coordinates (ρ, φ, z) : (radial distance, azimuthal angle, z-axis) [94Fel, Chap. 5].

$H_m^{(2)}$: m^{th} order Hankel function of the second kind [70Abr];
the change of convention in Sect. 3.1.1 includes: $H_m^{(2)} \Rightarrow H_m^{(1)}$ [94Fel, p. 487];
$\boldsymbol{\rho}$: radial position vector,
$\boldsymbol{e}_z$: unit vector along the z-axis.

3.1.3.1.3 Spherical vector wave

$$\boldsymbol{E} = E_0 \cdot (\boldsymbol{n}\times\boldsymbol{p})\times\boldsymbol{n}\ \cdot\ \frac{\exp(-i\, k_0\, \hat{n}\, r)}{r}\ , \tag{3.1.21}$$

$$\boldsymbol{H} = \frac{E_0}{c_0\mu_0}\cdot(\boldsymbol{n}\times\boldsymbol{p})\ \cdot\ \frac{\exp(-i\, k_0\, \hat{n}\, r)}{r} \quad (r \gg \lambda_0) \tag{3.1.22}$$

is the *far field* ($1/r^2$ and higher inverse power terms $\ll 1/r$-term) of an oscillating electric dipole ([99Bor, 94Leh, 75Jac]) with

E_0 : amplitude [V],
$\boldsymbol{p}$: unit vector of the dipole moment,
$\boldsymbol{n}$: unit vector pointing from dipole to spatial position,
r : radial distance.

3.1.3.2 Helmholtz equation

The approximative transition from the *vectorial* wave equation (3.1.4) to the Helmholtz equation (3.1.5) ([99Bor]) results in *scalar* solutions. E is called: "field" [72Mar], "complex displacement" or "scalar wave function" [99Bor], "disturbance" [95Bas, Vol. I].

3.1.3.2.1 Plane wave

$$E = E_0 \exp\{-\mathrm{i}\, k_0\, \hat{n}\, \boldsymbol{er} + \mathrm{i}\,\varphi\,.\} \tag{3.1.23}$$

For the parameters see (3.1.18).

3.1.3.2.2 Cylindrical wave

$$E = E_0\, H_0^{(2)}(k_0\, \hat{n}\, \rho) \quad (\rho > \lambda_0) \tag{3.1.24}$$

is the diverging field of a homogeneous line source [41Str, Chap. IV], [94Fel, Chap. 5]. For the parameters see (3.1.19).

3.1.3.2.3 Spherical wave

$$E = E_0 \cdot \frac{\exp(-\mathrm{i}\, k_0\, \hat{n}\, r)}{r} \quad (r > \lambda_0)\,, \tag{3.1.25}$$

parameters see (3.1.21).

3.1.3.2.4 Diffraction-free beams

3.1.3.2.4.1 Diffraction-free Bessel beams

Diffraction-free Bessel beams without transversal limitation are discussed in [05Hod, 91Nie, 88Mil].

$$E(x, y, z) = E_0 \cdot\ J_0(a\,\rho) \cdot\ \exp\{-\mathrm{i}\,\cos(\theta_\mathrm{B})\, k_0 z\} \tag{3.1.26}$$

with

E_0 : amplitude vector [V/m],
J_0 : zero-order Bessel function of the first kind [70Abr]; higher-order Bessel beams see [96Hal];
$\rho = \sqrt{x^2 + y^2}$: radial distance from the z-axis,
$a = k_0 \sin \Theta_\mathrm{B}$ [m^{-1}],
Θ_B : convergence angle of the conus of the plane wave normal to the z-axis, see Fig. 3.1.2.

3.1.3.2.4.2 Real Bessel beams

Real Bessel beams are limited by a finite aperture D of the optical elements needed or Gaussian beam illumination (Gaussian Bessel beams [87Gor]).

Methods of generation: axicons [85Bic] (Fig. 3.1.2), annular aperture in the focus of a lens [87Dur, 91Nie], holographic [91Lee] or diffractive [96Don] elements. Because of finite aperture diffraction the latter display approximately the shape of (3.1.26) with cutoff at a geometric determined radius r_N, which includes N maxima (Fig. 3.1.3) and different amplitude patterns in dependence on z.

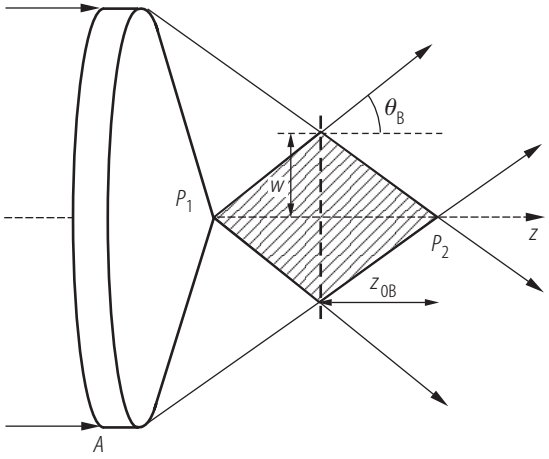

Fig. 3.1.2. Generation of a Bessel beam with help of an axicon A by a conus of plane-waves propagation directions.

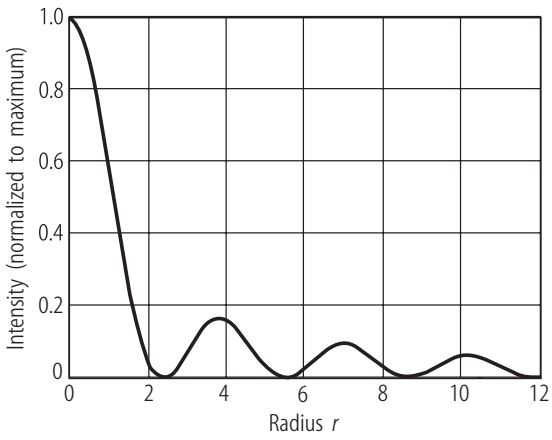

Fig. 3.1.3. Transversal intensity structure of a Bessel beam ($\propto J_0^2(r)$).

Advantage of Bessel beams: Large depth of focus $2\,z_{0B}$ between $P1$ and $P2$ in Fig. 3.1.2 (thin "needle of light") for measurement purposes.

Disadvantage: Every maximum in Fig. 3.1.3 contains in the corresponding circular ring nearly the same power as the central peak. High power loss occurs if the central part is used only [05Hod].

3.1.3.2.4.3 Vectorial Bessel beams

Vectorial Bessel beams are discussed in [96Hal].

3.1.3.3 Solutions of the slowly varying envelope equation

Gaussian beams are solutions of the *SVE-equation* (3.1.7) [91Sal, 96Ped, 86Sie, 78Gra], which is equivalent to paraxial approximation or Fresnel's approximation, see Sect. 3.1.4.

The *transition* from SVE-approximated Gaussian beams towards an exact solution of the wave equation in the non-paraxial range is given in a Lax-Wünsche series [75Lax, 79Agr, 92Wue]. For contour plots of the relative errors in the Gaussian beam volume see [97For, 97Zen].

The *vectorial field* of Gaussian beams is discussed in [79Dav, 95Gou], containing a Lax-Wünsche series; Gaussian beam in elliptical cylinder coordinates are given in [94Soi, 00Gou].

3.1.3.3.1 Gauss-Hermite beams (rectangular symmetry)

Elliptical higher-order Gauss-Hermite beam:

$$E_{mn}(x,y,z) = E_0\, U_m(x,z)\, U_n(y,z)\, \exp\{-\mathrm{i}\, k_0 z\}\ , \tag{3.1.27}$$

$$U_m(x,z) = \sqrt{\frac{w_{0x}}{w_x(z)}}\, H_m\left(\frac{\sqrt{2}\,x}{w_x(z)}\right)\, \exp\left\{-\frac{x^2}{w_x^2(z)} - \mathrm{i}\,\frac{k_0\, x^2}{2\, R_x(z)}\right\}\, \exp\{\mathrm{i}\,\varphi_m(z)\}\ , \tag{3.1.28}$$

$$U_n(y,z) = U_{m\Rightarrow n}(x\Rightarrow y, z) \tag{3.1.29}$$

with

w_{0x} : the $1/\mathrm{e}^2$-intensity waist radius,

$z_{0x} = \dfrac{\pi\, w_{0x}^2}{\lambda}$: the Rayleigh distance (half depth of focus),

$w_x(z) = w_{0x}\sqrt{1+\dfrac{z^2}{z_0^2}}$: the E_{00}-beam $1/\mathrm{e}^2$-intensity radius,

$R_x(z) = z\sqrt{1+\dfrac{z^2}{z_0^2}}$: the radius of curvature of the wavefront at position z,

$\varphi_m(z) = \left(\frac{1}{2}+m\right)\ \arctan\left(\frac{z}{z_0}\right)$: Gouy's phase, changing sign for the transition through $z=0$,

$H_m\left(\dfrac{\sqrt{2}}{w_x(z)}\right)$: the Hermite polynomial of order m [70Abr],

$H_0(\xi)=1\,,\ H_1(\xi)=2\,\xi\,,\ H_2(\xi)=4\,\xi^2-2\,,\ H_3(\xi)=8\,\xi^3-12\,\xi\,,\ H_4(\xi)=16\,\xi^4-48\,\xi^2+12\,,\ \ldots\,,$

$$\int_{-\infty}^{\infty} \mathrm{d}\,\xi \left\{\frac{\exp\left(-\xi^2/2\right)}{\sqrt{\sqrt{\pi}\, m!\, 2^m}} H_m(\xi)\right\}\left\{\frac{\exp\left(-\xi^2/2\right)}{\sqrt{\sqrt{\pi}\, n!\, 2^n}} H_n(\xi)\right\} = \delta_{mn}\ ,$$

$$\delta_{mn} = \begin{cases} 1 & \text{for } m=n \\ 0 & \text{for } m\neq n \end{cases}\quad (\textit{orthogonality relation})\ . \tag{3.1.30}$$

Example 3.1.4. Rotational symmetrical Gaussian fundamental mode (Gaussian beam):

Specialization of (3.1.27): $m=n=0\,,\ w_{0x}=w_{0y}=w_0\,,\ r=\sqrt{x^2+y^2}\,.$

$$E_{00}(r,z) = E_0\,\frac{w_0}{w(z)}\,\exp\left\{-\frac{r^2}{w^2(z)} - \mathrm{i}\,\frac{kr^2}{2R(z)}\right\}\exp\left\{\mathrm{i}\,\frac{1}{2}\arctan\frac{z}{z_0}\right\}\exp\{-\mathrm{i}\,kz\}\ , \tag{3.1.31}$$

$$w(z) = w_0\sqrt{1+\frac{z^2}{z_0^2}}\ ,\quad R(z) = z\sqrt{1+\frac{z_0^2}{z^2}}\ .$$

Properties of E_{00} (fundamental mode): The shape of the Gaussian E_{00}-beam is depicted in Fig. 3.1.4. *Parameters* of E_{00} in Fig. 3.1.4 are:

C : curves with constant amplitude decrease as $E(r,z)=E(0,z)/\mathrm{e}$
or constant intensity decrease as $I(r,z)=I(0,z)/\mathrm{e}^2$,
P : phase fronts with radius of curvature $R(z)$,

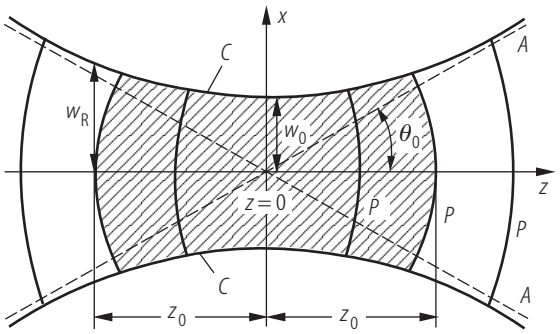

Fig. 3.1.4. Shape of the Gaussian E_{00}-beam.

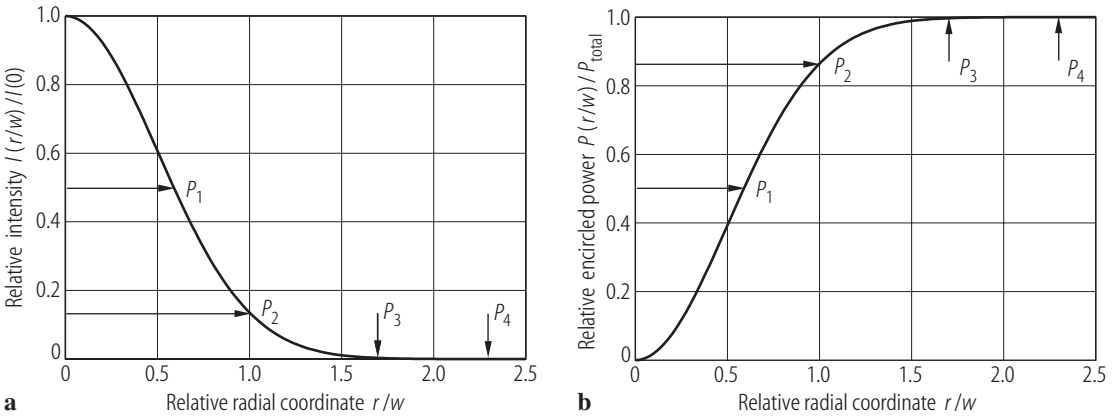

Fig. 3.1.5. (**a**) Cross section of a Gaussian beam perpendicular to the z-axis. (**b**) Power transmitted by a circular aperture with the relative radius r/w in a cross section.

Table 3.1.3. Characteristic points in Fig. 3.1.5.

Point in Fig. 3.1.5a, b	Relative abscissa r/w	Relative intensity, Fig. 3.1.5a	Relative transmission, Fig. 3.1.5b	Characterization
P_1	0.588	0.5	0.5	FWHM [a]
P_2	1	0.135	0.865	$1/e^2$-int. [b]
P_3	1.57	0.01	0.99	trunc. [c]
P_4	2.3	0.001	0.999	trunc. [d]

[a] Full width half maximum/2.
[b] $1/e^2$-intensity or 1/e-amplitude.
[c] Diffraction of E_{00}-beam by circular aperture ⇒ 17 % intensity ripple [86Sie, p. 667].
[d] Diffraction of E_{00}-beam by circular aperture ⇒ 1 % intensity ripple [86Sie, p. 667] (no essential effect of truncation).

w_0 : *beam waist*,
z_0 : *Rayleigh distance*, half of the *confocal parameter* $b = 2z_0$ (similarly to depth of focus in usual optics), that z-value, where the cross section $\pi w_R^2 = 2\pi w_0^2$ of the Gaussian beam has doubled in comparison with the waist,
$\Theta_0 = \lambda/(\pi w_0)$: $1/e^2$-intensity divergence angle toward the asymptotes A.

In Fig. 3.1.5a the cross section of a Gaussian beam perpendicular to the z-axis is given, in Fig. 3.1.5b the power transmitted by a circular aperture with the relative radius r/w in a cross section. Characteristic points in Fig. 3.1.5 are listed in Table 3.1.3.

Astigmatic and general astigmatic generalizations of the elliptical Gaussian beam: see Sect. 3.1.7.

3.1.3.3.2 Gauss-Laguerre beams (circular symmetry)

$$E_{lp}(r,\psi,z) = E_0 \exp\{-\mathrm{i}\,[kz - \varphi_{lp}(z)]\}\ \frac{w_0}{w(z)}\left(\frac{\sqrt{2}\,r}{w(z)}\right)^l L_p^l\left(\frac{2\,r^2}{w^2(z)}\right) \times \exp\left\{-\frac{r^2}{w^2(z)} - \mathrm{i}\,\frac{k\,x^2}{2\,R(z)}\right\}\left\{\begin{matrix}\cos(l\psi)\\ \sin(l\psi)\end{matrix}\right. \tag{3.1.32}$$

with

z : propagation direction,

r, φ : polar coordinates in the plane $\perp$ z-axis,

$z_0 = \dfrac{\pi w_0^2}{\lambda}$: the Rayleigh distance (half depth of focus),

$w(z) = w_0\sqrt{1 + \left(\dfrac{z}{z_0}\right)^2}$: the E_{00}-beam $1/\mathrm{e}^2$-intensity radius,

$R(z) = z\left\{1 + \left(\dfrac{z_0}{z}\right)^2\right\}$: the radius of curvature of the wavefront at position z,

$\varphi_{lp} = (2p + l + 1)\arctan\left(\dfrac{z}{z_0}\right)$: Gouy's phase,

L_p^l : Laguerre polynomial of degree p and order l [70Abr]:

$$L_0^l(\xi) = 1\,, \quad L_1^l(\xi) = (l+1) - \xi\,, \quad L_2^l(\xi) = \frac{(l+1)(l+2)}{2} - (l+2)\,\xi - \frac{1}{2}\,\xi^2\,,$$

$$L_3^l(\xi) = \frac{(l+3)(l+2)(l+1)}{6} - \frac{(l+3)(l+2)}{2}\,\xi + \frac{(l+3)}{2}\,\xi^2 - \frac{1}{6}\,\xi^3\ \ldots\,,$$

$$\int_0^\infty \mathrm{d}\,\xi\ \xi^l \exp(-\xi)\,L_p^l(\xi)\,L_q^l(\xi) = \delta_{pq}\,\frac{(l+p)!}{p!} \quad (\textit{orthogonality relation})\,, \tag{3.1.33}$$

$p!$: the factorial p.

- *Two degenerate mode patterns* are formed by the cos- and sin-terms in (3.1.32).
- $l = p = 0$ means the rotational symmetrical Gaussian beam E_{00}.
- The *symmetry* determines what system of Gauss-Laguerre polynomials or Gauss-Hermite polynomials is more appropriate for a wave field development.

3.1.3.3.3 Cross-sectional shapes of the Gaussian modes

In Fig. 3.1.6 intensity distributions of Gauss-Hermite modes E_{mn} are given (rectangular symmetry), in Fig. 3.1.7 intensity distributions of Gauss-Laguerre modes E_{pl} (circular symmetry).

Rectangular symmetry (Gauss-Hermite modes)

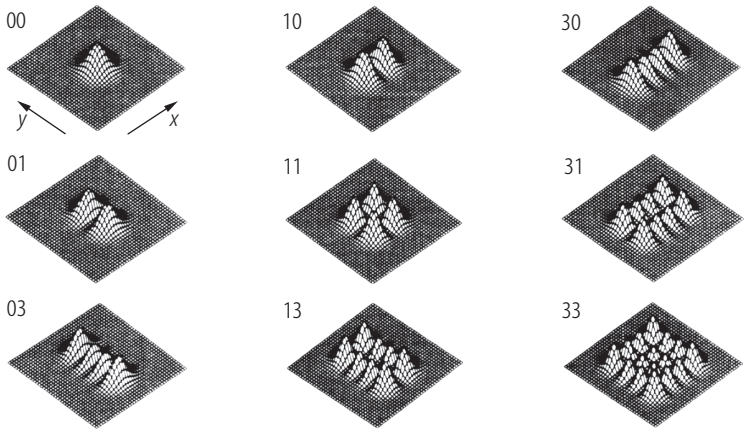

Fig. 3.1.6. Intensity distributions of Gauss-Hermite modes E_{mn}. The two digits at each distribution are m and n.

Circular symmetry (Gauss-Laguerre modes)

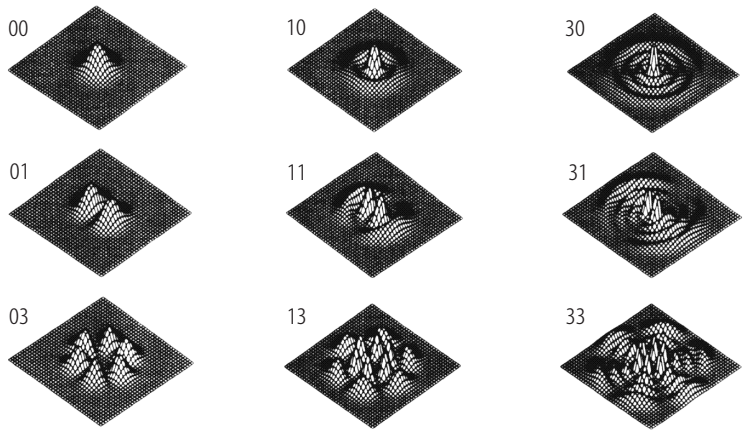

Fig. 3.1.7. Intensity distributions of Gauss-Laguerre modes E_{pl}. The two digits at each distribution are p and l. .

3.1.4 Diffraction

Diffraction of light by aperture rims or amplitude and phase modifications inside the aperture:

- Solutions of Maxwell's equations taking into account the material properties of the aperture:
  - special cases: exact solutions [99Bor, 86Sta],
  - mostly: numerical solutions.
- Starting with a field near the aperture with reasonable assumptions for this field or its measurement: large variety of methods for different ranges of validity [99Bor, 86Sta, 61Hoe].

3.1.4.1 Vector theory of diffraction

- *Vectorial generalization* of Kirchhoff's theory: Given $\boldsymbol{E}$ and $\boldsymbol{H}$ in an aperture $\Rightarrow$ $\boldsymbol{E}$ and $\boldsymbol{H}$ in the volume by Stratton-Chu Green's function representation [23Kot, 41Str, 86Sol, 91Ish].
- *Two-dimensional problem* and meridional incidence of light [61Hoe]: Separation of the polarizations $\boldsymbol{E}$ parallel and $\boldsymbol{E}$ perpendicular to the plane of incidence for half plane [99Bor], slit [99Bor], gratings [80Pet], and volume gratings [69Kog, 81Sol, 81Rus].

3.1.4.2 Scalar diffraction theory

Two sources of scalar diffraction theory are:

- Transition from *vectorial* theory to *scalar* theory: [99Bor, 86Sol]. The information about the polarization is lost.
- Mathematical formulation and generalization of *Huygens' principle*: Each point on a wavefront may be regarded as a source of secondary waves, and the position of the wavefront at a later time is determined by the envelope of these secondary waves.

In Table 3.1.4 *diffraction formulae* with fields given near the diffraction aperture are listed. Figures 3.1.8 and 3.1.9 are related to Table 3.1.4.

Remarks on the formulae of Table 3.1.4:

(3.1.37): Approximation of (3.1.34): Huygens' principle with an additional directional factor (Fresnel).

(3.1.38): Approximation of (3.1.36): Huygens' principle with a modified directional factor.

(3.1.39): *Fresnel's approximation* (= paraxial approximation). The approximation conditions from (3.1.34) to (3.1.39) resp. (3.1.40) are explained in [96For, 86Sta, 87Ree].

Fresnel's approximation: The condition $N_{\mathrm{F}}(a/d)^2/4 \ll 1$ [91Sal] is valid for sharp-edged apertures A, but it is weakened for the transmission of Gaussian-beam-like fields [86Sie, p. 635] or Gaussian-like soft apertures. Fresnel's approximation describes the propagation of the field from plane $z = 0$ to plane $z = z$. This transformation can be cascaded to describe complex systems and is an often used *tool in paraxial propagation* of radiation (Sect. 3.1.4.5.2).

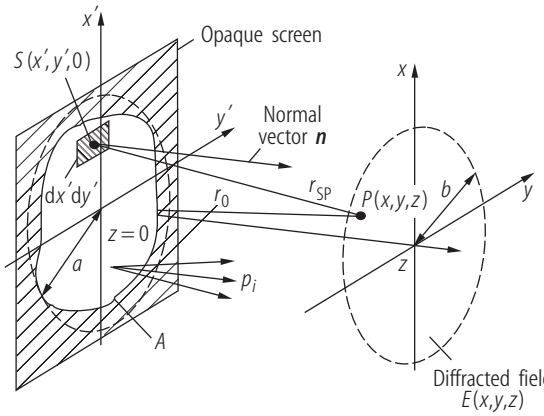

Fig. 3.1.8. Diffraction at an aperture A with source terms $E(x', y', 0)$ and/or $\frac{\partial}{\partial z}E(x', y', z)\big|_{z=0}$, respectively, and a or b the maximum radial distances of source S or image point P, respectively. p_i symbolizes different plane waves for (3.1.41)–(3.1.43).

Table 3.1.4. *Diffraction formulae* with fields given near the diffraction aperture (r_{SP} : see Fig. 3.1.8).

Integrals	Formula		Restrictions	Ref.
Rayleigh-Sommerfeld of 1st kind	$E_{RS1}(x,y,z) = -\frac{1}{4\pi}\iint\limits_A E(x',y',0)\,\frac{\partial}{\partial z}\left(\frac{\exp(-\mathrm{i}\,k r_{SP})}{r_{SP}}\right)\mathrm{d}\,x'\,\mathrm{d}\,y'$	(3.1.34)	$r_{SP} > \lambda_0$, plane aperture	[99Bor] [86Sta]
Rayleigh-Sommerfeld of 2nd kind	$E_{RS2}(x,y,z) = -\frac{1}{2\pi}\iint\limits_A \left[\frac{\partial\,E(x',y',z')}{\partial\,z}\right]_{z'=0}\frac{\exp(-\mathrm{i}k r_{SP})}{r_{SP}}\,\mathrm{d}\,x'\,\mathrm{d}\,y'$	(3.1.35)	$r_{SP} > \lambda_0$, plane aperture	
Fresnel-Kirchhoff	$E_{FK}(x,y,z) = \frac{1}{2}\left[E_{RS1}(x,y,z) + E_{RS2}(x,y,z)\right]$	(3.1.36)	$r_{SP} > \lambda_0$, curved aperture	
Rayleigh-Sommerfeld 1st kind approx.	$E_{RS1a}(x,y,z) = \frac{1}{\mathrm{i}\,\lambda}\iint\limits_A E(x',y',0)\,\frac{\exp(-\mathrm{i}\,k r_{SP})}{r_{SP}}\,\cos(n, r_{SP})\,\mathrm{d}\,x'\,\mathrm{d}\,y'$	(3.1.37)	$r_{SP} \gg \lambda_0$	
Fresnel-Kirchhoff approximation, refers to Fig. 3.1.8	$E_{FKa}(x,y,z) = \frac{1}{\mathrm{i}\,\lambda}\iint\limits_A E(x',y',0)\,\frac{\exp(-\mathrm{i}\,k r_{SP})}{r_{SP}}\cdot\frac{1+\cos(n, r_{SP})}{2}\,\mathrm{d}\,x'\,\mathrm{d}\,y'$	(3.1.38)	$r_{SP} \gg \lambda_0$	
Fresnel's approximation, refers to Fig. 3.1.8	$E_{Fre}(x,y,z) = \frac{\mathrm{i}\,\exp(-ikz)}{\lambda d}\iint\limits_A E(x',y',0)\,\exp\left\{-\mathrm{i}\,\pi\,\frac{(x-x')^2+(y-y')^2}{\lambda\,z}\right\}\mathrm{d}\,x'\,\mathrm{d}\,y'$	(3.1.39)	$z \gg \lambda_0$	[99Bor] [96For] [97For] [87Ree] [86Sta]

(continued)

Table 3.1.4 continued.

Integrals	Formula	Restrictions	Ref.
Fraunhofer far-field approximation, refers to Fig. 3.1.8	$E_{\mathrm{Fra}}(x,y,z) = \frac{\mathrm{i}\exp(-\mathrm{i}kz)\,p}{\lambda z} \iint\limits_A E(x',y',0)\ \exp\left\{\mathrm{i}\,2\pi\frac{xx'+yy'}{\lambda z}\right\}\mathrm{d}x'\,\mathrm{d}y'$ (3.1.40) with the additional phase term $p = \begin{cases} 1 & \text{for} \quad \frac{b^2}{\lambda z} \ll 1 \\ \exp\left\{-\mathrm{i}\,\pi\,\frac{x^2+y^2}{\lambda z}\right\} & \text{otherwise} \end{cases}$	$\frac{a^2}{\lambda d} \ll 1$	[99Bor] [68Goo] [96For] [97For] [86Sta]
Plane-wave representation (also: angular-spectrum representation), refers to Figs. 3.1.8 and 3.1.9	2-D Fourier transform (see remark on (3.1.40)) of the source distribution E_{s} in plane $z = 0$: $A_0(f_x,f_y) = \int\limits_{-\infty}^{\infty}\int\limits_{-\infty}^{\infty} E_{\mathrm{s}}(x',y',0)\exp\left\{\mathrm{i}\,2\,\pi\,(f_x x' + f_y y')\right\}\mathrm{d}x'\,\mathrm{d}y'$, (3.1.41) propagation of plane waves with the spatial frequencies f_x and f_y along the z-direction by distance z: $\exp\{-\mathrm{i}\,2\,\pi\,(f_x x + f_y y\} \Rightarrow \exp\left\{-\mathrm{i}\,2\,\pi\,(f_x x + f_y y + \sqrt{1/\lambda^2 - f_x^2 - f_y^2}\ z)\right\}$, (3.1.42) addition of plane waves at distance z: $E(x,y,z) = \int\limits_{f_x^2+f_y^2<1/\lambda^2}\int A_0(f_x,f_y)\exp\left\{-\mathrm{i}\,2\,\pi\,\left(f_x x + f_y y + \sqrt{1/\lambda^2 - f_x^2 - f_y^2}\ z\right)\right\}\mathrm{d}f_x\,\mathrm{d}f_y$, (3.1.43) equivalent to (3.1.34) [97For]	$r_{\mathrm{SP}} > \lambda_0$	[91Sal] [78Loh] [86Sta] [97For] [99Bor]
Far field in the focal plane of a lens, refers to Fig. 3.1.9	$E_{\mathrm{P}}(x,y) = \frac{\mathrm{i}\,p}{\lambda f}\int\limits_{-\infty}^{\infty}\int\limits_{-\infty}^{\infty} E_{\mathrm{S}}(x',y')\ \exp\left\{\mathrm{i}\,2\,\pi\,\left(\frac{x}{\lambda f}\,x' + \frac{y}{\lambda f}\,y'\right)\right\}\mathrm{d}x'\,\mathrm{d}y'$, (3.1.44) $p = \exp\left(\mathrm{i}\,\pi\,\frac{(x^2+y^2)\,(d-f)}{\lambda\,f^2}\right)$ (3.1.45)	$d, f \gg \lambda$	[91Sal]

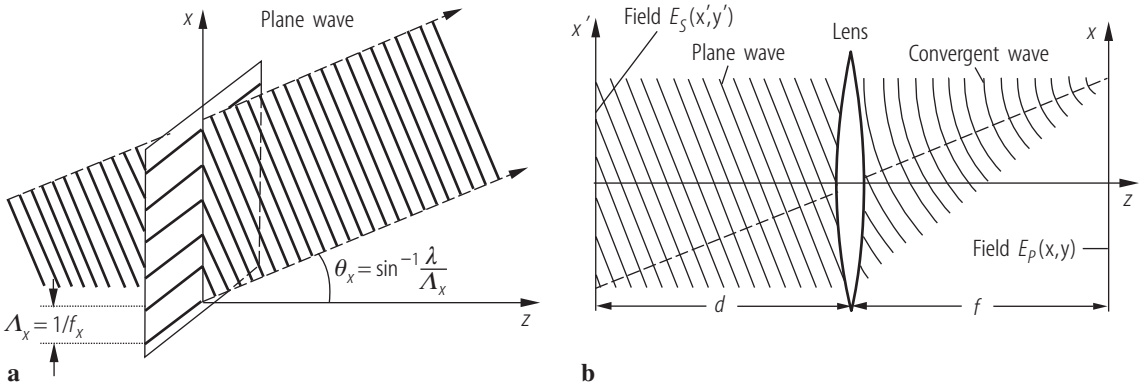

Fig. 3.1.9. (**a**) *Spatial frequencies* of a plane wave with propagation direction Θ_x with respect to the plane $x = 0$ (and Θ_y analogously) are f_x and f_y with $\Theta_x = \sin^{-1}(\lambda f_x) \approx \lambda f_x$ and $\Theta_y = \sin^{-1}(\lambda f_y) \approx \lambda f_y$ ($\approx$: paraxial approximation). (**b**) Generation of the far field in the focal plane of a lens: The Fourier transformation ($d = f$) is changed by an additional phase term for $d \neq f$ with d: distance, f: focal length.

(3.1.40): *Fraunhofer's approximation*

– *Fresnel number*:

$$N_\mathrm{F} = a^2/\lambda z \; . \tag{3.1.46}$$

  – Validity of Fraunhofer's approximation: $N_\mathrm{F} \ll 1$.
  $p \neq 1$ (parabolic phase): the *intensity* of diffracted light is the square of the *modulus* of the Fourier transform of $E(x, y, 0)$ only.
  – Additional condition with second Fresnel number $N_{\mathrm{F}'} = b^2/\lambda z \ll 1$:
  $E(x, y, z)$ is the *Fourier transform* of $E(x, y, 0)$ in dependence on the spatial frequencies $f_x \approx (x/z)/\lambda \approx \Theta_x/\lambda$ and $f_y \approx (y/z)/\lambda \approx \Theta_y/\lambda$.

– *Different conventions* on the *spatial Fourier transform* $F(f_x)$ of a spatial distribution $f(x)$:

  – The convention of the plane-wave structure $\exp(\mathrm{i}\,kx - \mathrm{i}\,\omega\,t)$ is connected with the determination of $F(f_x)$ by

$$F(f_x) = \int_{-\infty}^{\infty} \mathrm{d}\,x\, f(x)\, \mathrm{e}^{-\mathrm{i}\,2\pi\, f_x x}$$

  [68Goo, 68Pap, 78Loh, 78Gas, 93Sto, 05Hod].
  – The plane-wave structure $\exp(\mathrm{i}\,\omega\,t - \mathrm{i}\,kx)$ can be combined with

$$F(f_x) = \int_{-\infty}^{\infty} \mathrm{d}\,x\, f(x)\, \mathrm{e}^{\mathrm{i}\,2\pi\, f_x x}$$

  [71Col, 73Men, 92Lug], but

$$F(f_x) = \int_{-\infty}^{\infty} \mathrm{d}\,x\, f(x)\, \mathrm{e}^{-\mathrm{i}\,2\pi\, f_x x}$$

  is defined also in [88Kle, 91Sal, 95Wil, 96Ped].

– *Different approximations* in (3.1.37) and (3.1.38):

$$r_{SP} \approx r_0 + \frac{2x\xi - \xi^2 + 2y\eta - \eta^2}{2r_0}$$

[99Bor, 68Pap, 78Gra] with r_0 from Fig. 3.1.8 versus

$$r_{SP} \approx z + \frac{2xx' - x'^2 + 2yy' - y'^2}{2z}$$

(references on lasers: [86Sie, 05Hod], optoelectronics: [68Goo, 72Mar, 91Sal]) for *grating diffraction*: The sine of the diffraction angle $\sin \Theta_x = x/r_0$ is derived from principle and not by a postpositive reasoning of the paraxial range $x/z = \tan \Theta_x \approx \sin \Theta_x$. x/z should be "translated" into $\sin \Theta_x$ for better approximation.

(3.1.41)–(3.1.43): *Plane-wave spectrum or angular-spectrum representation* (also Rayleigh-Sommerfeld-Debye diffraction theory) [78Loh, 99Pau] is the plane-wave formulation of (3.1.34) [78Loh, 97For]. Application: see *Fourier optics* [68Goo, 83Ste, 93Sto].

(3.1.44), (3.1.45): *Generation of the far field in the focal plane of a lens*: $d \neq f$ (object is outside the object-side focal plane) $\Rightarrow$ additional phase term p to the pure (inverse) Fourier transform ($d = f$), similarly to (3.1.40).

Applications: generation of the spectrum of a function, possibility of mathematical operations in the Fourier-space with complex filtering masks, correlation and convolution.

Another important diffraction theory

Diffraction theory after *Young, Maggi, Rubinowicz* [66Rub, 99Pau]: The light in point P of Fig. 3.1.8 results from the unperturbed light and local waves, which are emitted by the edge of the aperture A. Therefore, a line integral is to be calculated [99Pau]. There is an equivalence with Fresnel-Kirchhoff's theory.

3.1.4.3 Time-dependent diffraction theory

Two formulations of the time-dependent treatment of diffraction are possible:

1. A general Fresnel-Kirchhoff's integral formula exists for *time-dependent source functions* in the aperture A, see [99Bor, 99Pau].
2. Used more often now [96Die, 99Pau]: The time-dependent source functions are decomposed into a *superposition of monochromatic fields*. The diffracted field is calculated for every monochromatic component by the stationary diffraction given above. The superposition of all diffracted monochromatic components yields the time-dependent diffracted field.

3.1.4.4 Fraunhofer diffraction patterns

3.1.4.4.1 Rectangular aperture with dimensions $2a \times 2b$

In Fig. 3.1.10 the geometry of the diffraction from a rectangular aperture $2a \times 2b$ is shown. The x-part of the diffraction pattern in Fig. 3.1.10 is given in Fig. 3.1.11. In Table 3.1.5 the zeros and maxima of the intensity distribution are listed.

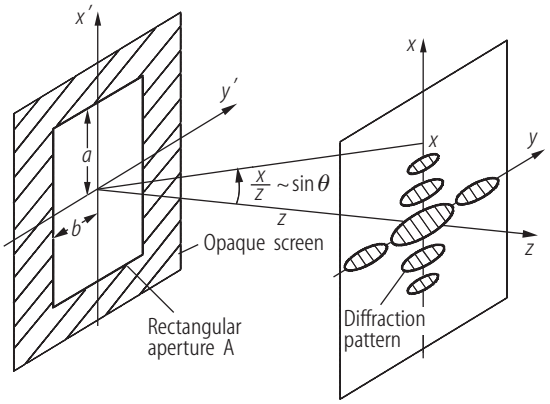

Fig. 3.1.10. Geometry of the diffraction from a rectangular aperture $2a \times 2b$.

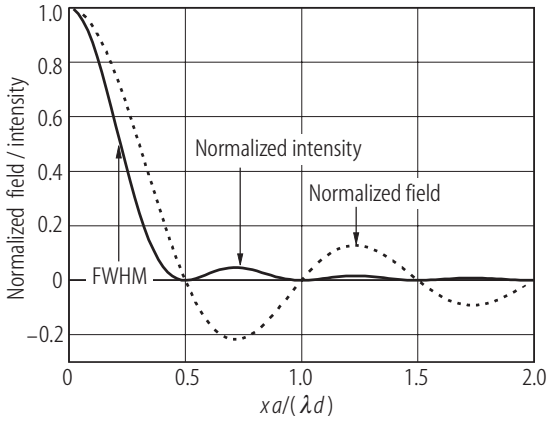

Fig. 3.1.11. x-part of the diffraction pattern in Fig. 3.1.10. This is the diffraction pattern of a slit. For more exact electromagnetic solutions of a slit see [61Hoe, p. 266].

Table 3.1.5. Zeros and maxima of the intensity distribution.

Number n	$xa/\lambda z$	I_n/I_0
0	0	1
FWHM	2×0.221	0.5
1	0.5	0
1	0.715	0.0472
2	1	0
2	1.230	0.0168
3	1.5	0
3	1.735	0.0083
4	2	0
4	2.239	0.0050

Field distribution:

$$E(x,y,z) = \frac{4\,a\,b}{\mathrm{i}\,\lambda\,z}\; E_0\; \exp\left\{-\mathrm{i}\,k\,\left(z + \frac{x^2+y^2}{2\,z}\right)\right\}\; \mathrm{sinc}\left\{\frac{2\,\pi\,a\,x}{\lambda\,z}\right\}\; \mathrm{sinc}\left\{\frac{2\,\pi\,b\,y}{\lambda\,z}\right\} \tag{3.1.47}$$

with $\mathrm{sinc}(x) = \dfrac{\sin x}{x}$ and E_0 the electric-field amplitude .

Intensity:

$$I(x,y,z) = I(0,0,z)\; \mathrm{sinc}^2\left\{\frac{2\,\pi\,a\,x}{\lambda\,z}\right\}\; \mathrm{sinc}^2\left\{\frac{2\,\pi\,b\,y}{\lambda\,z}\right\}\;. \tag{3.1.48}$$

If the Fraunhofer diffraction is observed in the focal plane, z has to be replaced by f.

3.1.4.4.2 Circular aperture with radius a

The circular aperture with radius a is discussed in [61Hoe, p. 453]. In Fig. 3.1.12 diffraction by a circular aperture is shown. In Fig. 3.1.13a the diffracted field and intensity and in Fig. 3.1.13b the encircled energy in the diffraction plane with a circular screen are given. The zeros and maxima of intensity for diffraction by a circular aperture are listed in Table 3.1.6.

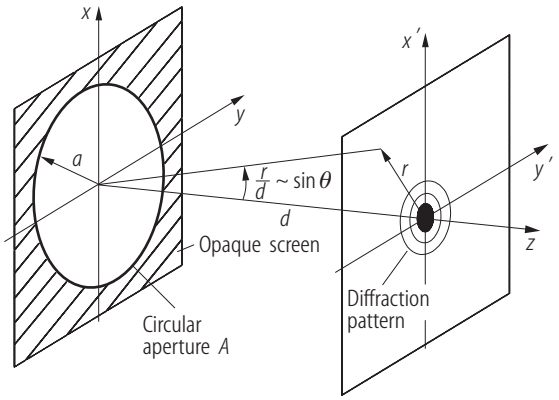

Fig. 3.1.12. Diffraction by a circular aperture.

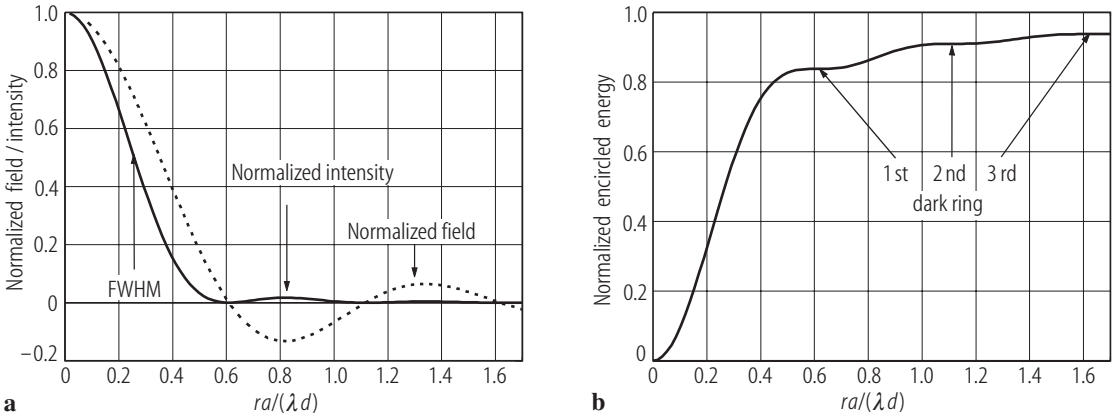

Fig. 3.1.13. (**a**) Diffracted field and intensity. (**b**) Encircled energy in the diffraction plane with a circular screen.

Table 3.1.6. Zeros and maxima of intensity for diffraction by a circular aperture.

Number n	$r_n a/(\lambda d)$	I_n/I_0
0	0	1
FWHM	2×0.257	0.5
1	0.610	0
1	0.817	0.0175
2	1.117	0
2	1.340	0.00415
3	1.619	0
3	1.849	0.00160
4	2.121	0
4	2.355	0.00078

Field distribution:

$$E(r,z) = \frac{\pi a^2}{\mathrm{i}\lambda z}\, E_0 \exp\left\{-\mathrm{i}\, k\left(z + \frac{kr^2}{2z}\right)\right\}\left\{2\,\frac{J_1\left[2\pi a\, r/(\lambda z)\right]}{2\pi a\, r/(\lambda z)}\right\} \tag{3.1.49}$$

with E_0 the electric-field amplitude and r the radius in the far-field plane.

Intensity:

$$I(r) = I(0,z)\left\{2\,\frac{J_1[2\pi a\, r/(\lambda z)]}{2\pi a\, r/(\lambda z)}\right\}^2 . \tag{3.1.50}$$

3.1.4.4.2.1 Applications

Airy's disc:

$$r_{1\,\mathrm{Airy}} = 0.610\,\lambda/\sin\sigma\ , \tag{3.1.51}$$

1st-minimum radius of the intensity distribution in the focal plane of an aberration-free lens (Lommel 1885, Debye 1909, [86Sta, 99Bor]): Substitute in (3.1.50) $a/z \Rightarrow \sin\sigma$ (numerical aperture = sinus of the intersection angle σ with optical axis in the focal point, *generally*: *image point*) and $r = r_{1\,\mathrm{Airy}}$ as above.

Annular aperture: obscuration of the central part in the circular aperture A of Fig. 3.1.12:

- Reduction of the central diffraction maximum width by ≈ 20 %.
- Increase of secondary maximum by factor ≈ 7.
- See Bessel beams, Sect. 3.1.3.2.4, [05Hod].

3.1.4.4.3 Gratings

Grating equation:

$$\sin\alpha + \sin\beta = m\,\frac{\lambda}{g} \tag{3.1.52}$$

with

α: angle of incidence (see Fig. 3.1.14),
β: diffraction angle,
g: grating constant (grating period, groove distance),
m: order of diffraction. *Convention* [82Hut, p. 25] often used: If the diffraction order is on the same side with the zero order ($m = 0$) as the grating normal: $m > 0$, otherwise $m < 0$. In Fig. 3.1.14, the directions of the +1st transmitted order and the grating normal (dashed and dotted lines) are on the same side of the 0th transmitted order. Therefore $m = 1 > 0$.

Slit factor: represents the diffraction by a single slit of the grating. Its form regulates the energy distribution between the different orders m [82Hut, 99Bor]. For the real phase and reflection gratings, it is substituted by the *diffraction efficiency* curves in dependence on α or λ. There is an extreme diversity of cases. Catalogs of such curves: see [80Pet, 97Loe].

Theoretical spectral resolution of a grating:

$$R_{\mathrm{theor}} = \lambda/(\Delta\lambda) = m\,N = W\,(\sin\alpha + \sin\beta)/\lambda \tag{3.1.53}$$

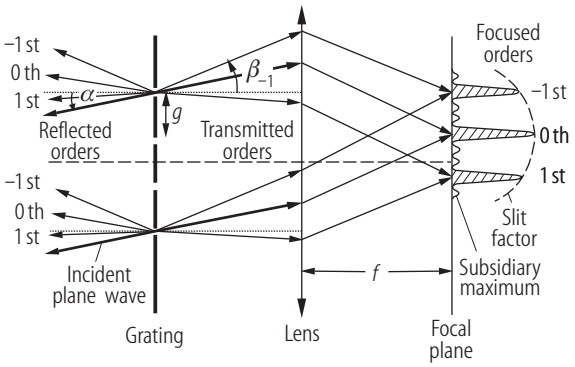

Fig. 3.1.14. Reflected and transmitted orders of a grating, here with $N = 4$ slits. The far-field distribution is *visualized* after focusing by an *ideal* lens. Between the main maxima occur $N - 2$ subsidiary maxima. The dashed envelope is the *slit factor*.

with

N : number of grooves of the grating,
W : width of the grating,
α, β : see (3.1.52).

Real resolution contains theoretical resolution and the aberrations of the optical elements for collimation and focusing of the grating-diffracted plane waves or by the aberrations of the *concave gratings* with imaging properties. [87Chr, 82Hut].

Holographical gratings [82Hut] show lower disturbations than mechanically produced gratings (application: external laser resonators).

Blazed gratings diffract light into an order m wanted with more than 60–90 % over one octave of wavelengths [80Pet, 82Hut, 97Loe].

Volume gratings: [81Sol, 81Rus].

Mountings of spectral devices: [82Hut].

3.1.4.5 Fresnel's diffraction figures

Fresnel's approximation is given in (3.1.39) in Table 3.1.4.

3.1.4.5.1 Fresnel's diffraction on a slit

In Fig. 3.1.15 Fresnel's diffraction pattern of a slit with width $2a$ is shown.

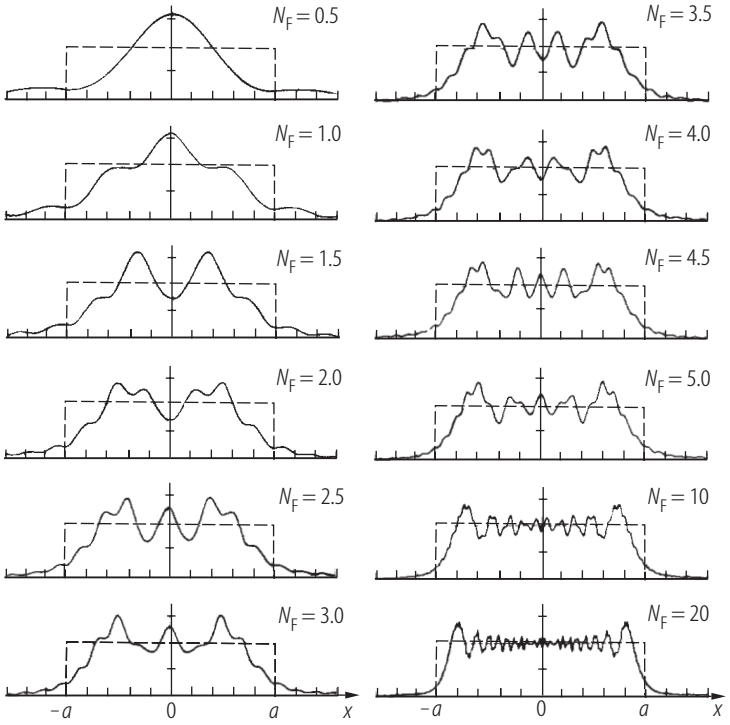

Fig. 3.1.15. Fresnel's diffraction pattern of a slit with width $2a$ (see Fig. 3.1.10 with $b \Rightarrow \infty$). *Fresnel's number* $N_F = a^2/(\lambda z)$ is the essential parameter to characterize the transition from far-field (Fraunhofer) approximation ($N_F < 0.2 \ldots 0.5$) to near-field (Fresnel) approximation ($N_F > 0.5$). $N_F = 0.5$: one central maximum only, $N_F = 3$: three maxima, $N_F = N$: N maxima. *Hard-edge* diffraction results in a ripple in the near field, which can be avoided by *soft apertures*, for instance Gaussian-like [86Sie] (apodization in optics [99Bor]). Figure after [86Sie, p. 721].

3.1.4.5.2 Fresnel's diffraction through lens systems (paraxial diffraction)

Given: a system of lenses and the field distribution $E(x, y)$ to be propagated.

The *sequence of steps* easily taken is:

- Given: $E(x, y)$ in the plane $z = 0$. Required: the field in the plane $z = z$. Solution: (3.1.39).
- Given: $E(x, y)$ in the plane $z = 0$ and near to this plane a lens. Required: the field in the plane $z = z$. Solution: modification of (3.1.39) by an additional factor $L(x', y')$ to:

$$E_{\mathrm{Fre}}(x, y, z) = \frac{\mathrm{i}\,\exp\{-\mathrm{i}\,kz\}}{\lambda d} \iint\limits_A E(x', y', 0)\; L(x', y') \times \exp\left\{-\mathrm{i}\,\pi\,\frac{(x - x')^2 + (y - y')^2}{\lambda\, z}\right\} \mathrm{d}\,x'\,\mathrm{d}\,y'\,, \tag{3.1.54}$$

$$L(x', y') = p(x', y')\;\exp\{-\mathrm{i}\,kn\,t_{\mathrm{L}}\}\;\exp\left\{\frac{\mathrm{i}\,k(x'^2 + y'^2)}{2f}\right\} \tag{3.1.55}$$

with

n : refractive index of the lens,
t_{L} : thickness of the lens,
f : focal length of the lens,
$p(x', y')$: amplitude part, which can describe a marginal aperture or a Gaussian apodization.

A general complex function $L(x', y')$ can model diffractive optical elements.

Cases of integration:

- No transversal limitations (without stops) and quadratic arguments of the exponential functions due to analytical results. The *Collins integral* is the closed form of such a calculation (see Sect. 3.1.7.4).
- One stop (finite integration limits): The result includes the error function [70Abr].
- Two and more finite integration limits are not useful. Then, (commercial) numerical field propagation programs through systems should be consulted.

Examples: [68Goo, 91Sal, 71Col, 85Iiz, 92Lug, 68Pap].

The *Beam Propagation Method (BPM)* in integrated optics (many "infinitely thin lenses") is the generalization of this method [95Mae, 91Spl, 99Lau, 98Hec].

3.1.4.6 Fourier optics and diffractive optics

Fourier optics results from the transformation of the temporal frequency methods of electrical engineering to spatial frequency methods in optics, see Figs. 3.1.9, 3.1.10 and (3.1.41), (3.1.43), (3.1.44).

References: principles of Fourier optics: [68Goo, 78Loh, 83Ste, 85Iiz, 89Ars, 93Sto, 98Hec, 99Lau], filtering: [92Lug], filtering in connection with holography: [96Har, 71Col], noise suppression: [91Wyr].

Example 3.1.5. Spatial spectral filtering

In Fig. 3.1.16 low-pass filtering of a laser beam with a four-f-setup is shown.

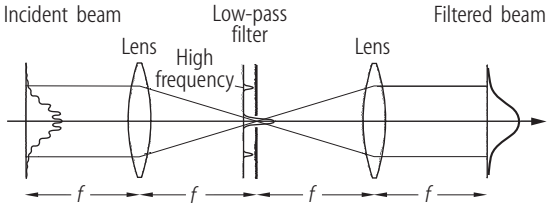

Fig. 3.1.16. Low-pass filtering of a laser beam with a four-f-setup [92Lug]. The mask is a low-pass filter, which transmits a zero mode only and suppresses the higher modes. The incident beam can also be modified by a transmission element which changes amplitude and phase.

Diffractive optical elements influence the propagation of light with help of amplitude- and/or phase-changing microstructures whose dimensions are of the order of the wavelength mostly. They extend the classical means of optical design. References: [67Loh, 84Sch, 97Tur, 00Tur, 00Mey, 01Jah].

Example 3.1.6.

- *Gratings* generated by mechanical or interference ruling [69Str, 67Rud] on either plane or concave substrates for the combination of dispersive properties with imaging [82Hut, 87Chr].
- *Fresnel's zone plates* acting as microoptic lenses of [97Her].
- *Mode transformation optics* ("modane") for transformation and filtering of modes of a laser [94Soi].
- Generation of theoretical ideal wavefronts for *optical testing* with interferometrical methods [95Bas, Vol. II, Chap. 31].
- Mode-discriminating and emission-forming elements in resonators [94Leg, 97Leg, 99Zei].

For pure imaging applications, refracting surfaces are still preferred, even in the micro-range [97Her]. Tasks with special dispersion requirements and special optical field transformations are the main application of the diffractive elements with increasing share.

The technology of dispersion compensation and weight reduction in large optical systems by special diffractive elements is partially solved, now.

3.1.5 Optical materials

Medium with absorption:

$$\hat{\varepsilon}_\mathrm{r} = \hat{n}^2 \tag{3.1.56}$$

with

$\hat{\varepsilon}_\mathrm{r}$: complex relative dielectric constant (or tensor),
$\hat{n}$: complex refractive index,

weakly absorbing isotropic medium:

$$\alpha \ll k_0 \;:\quad \hat{n} = n - \mathrm{i}\, k_\mathrm{e} = n - \mathrm{i}\, n\, \kappa = n - \mathrm{i}\, \frac{\alpha}{2\, k_0}\ , \tag{3.1.57}$$

damped plane wave (unity field amplitude):

$$\begin{aligned} \exp\{-\mathrm{i}\, kz\} &= \exp\{-\mathrm{i}\, k_0 (n - \mathrm{i}\, \kappa)\, z\} \exp\left\{-\mathrm{i}\, k_0 \left(n - \mathrm{i}\, \frac{\alpha}{2\, k_0}\right) z\right\} \\ &= \exp\left\{-\mathrm{i}\, k_0 z - \frac{\alpha}{2} z\right\}\ , \end{aligned} \tag{3.1.58}$$

intensity:

$$I(z) = I(0)\,\exp\{-\alpha\, z\} \quad (\textit{Lambert-Beer-Bouguer's law}\ ), \tag{3.1.59}$$

amplification in pumped media:

$$I(z) = I(0)\,\exp\{g\, z\} \tag{3.1.60}$$

with

α [m^{-1}]: (linear) *absorption constant* (standard definition [95Bas, Vol. II, Chap. 35], [99Bor, 91Sal, 96Yar, 05Hod]) or extinction constant or attenuation coefficient,
g [m^{-1}] : *gain*,
k_e [m^{-1}]: [88Yeh, 95Bas] (or κ [m^{-1}]: [99Bor, 04Ber]) *extinction coefficient*, attenuation index.

Different *convention* after (3.1.6): α, g, k_e and κ are defined with other signs, for example $\hat{n} = n\,(1 + i\,\kappa)$ if the other time separation (1^{st} convention) is used [99Bor, Chap. 13], [95Bas, Vol. I, Chap. 9].

Measurement of α: see [85Koh, 04Ber, 82Bru], [90Roe, p. 34], [95Bas, Vol. II, Chap. 35].

3.1.5.1 Dielectric media

In Fig. 3.1.17 the real- and imaginary part of the refractive index in the vicinity of a resonance in the UV are shown.

Single-resonance model for low-density media [99Bor, 96Ped]:

$$\begin{aligned}\hat{n} = n - i\,k_e &= 1 + \frac{N\,e^2}{2\,\varepsilon_0 m\,(\omega_0^2 - \omega^2 + i\,\gamma\,\omega)} \\ &= \left\{1 + \frac{N\,e^2\gamma\,\left(\omega_0^2 - \omega^2\right)}{2\,\varepsilon_0 m\,[(\omega_0^2 - \omega^2)^2 + \gamma^2\,\omega^2]}\right\} - i\,\left\{\frac{N e^2 \gamma\,\omega}{2\,\varepsilon_0 m\,[(\omega_0^2 - \omega^2)^2 + \gamma^2\,\omega^2]}\right\}\end{aligned} \tag{3.1.61}$$

with

$e = -1.602 \times 10^{-19}$ C: elementary charge,
$m = 9.109 \times 10^{-31}$ kg: mass of the electron,
$\omega = 2\,\pi\,\nu$ [s^{-1}]: circular frequency of the light,
ω_0 [s^{-1}]: circular resonant frequency of the electron,

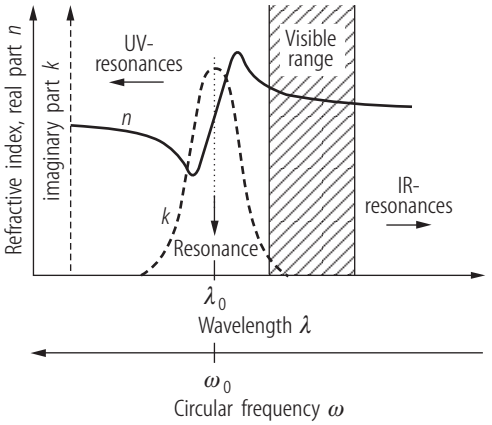

Fig. 3.1.17. Real- and imaginary part of the refractive index in the vicinity of a resonance in the UV. The principal shape is explained by the classical oscillator model after J.J. Thomson, P. Drude, and H.A. Lorentz [99Bor, 88Yeh].

γ [s^{-1}]: damping coefficient,
N [m^{-3}]: density of molecules,
$\varepsilon_0 = 8.8542 \times 10^{-12}$ As/Vm: electric permittivity of vacuum.

Examples see [96Ped, 88Kle], generalization to dense media see [96Ped, 88Kle, 99Bor].

The *Kramers-Kronig relation* connects $n(\omega)$ with $k(\omega)$ [88Yeh].

3.1.5.2 Optical glasses

Dispersion formula [95Bac]:

$$n^2(\lambda) = 1 + \frac{B_1\lambda^2}{\lambda^2 - C_1} + \frac{B_2\lambda^2}{\lambda^2 - C_2} + \frac{B_3\lambda^2}{\lambda^2 - C_3} \quad (\textit{Sellmeier's formula}) \,. \tag{3.1.62}$$

The dimensions of the constants are given in example 3.1.7. The available wavelength range is given by the transmission limits, usually.

Example 3.1.7. [96Sch]: Glass N-BK7: λ [µm], $B_1 = 1.03961212$, $B_2 = 2.31792344 \times 10^{-1}$, $B_3 = 1.01046945$, $C_1 = 6.00069867 \times 10^{-3}$ [μm^2], $C_2 = 2.00179144 \times 10^{-2}$ [μm^2], $C_3 = 1.03560653 \times 10^2$ [μm^2], $n(0.6328\ \mu m) = 1.51509$, $n(1.06\ \mu m) = 1.50669$.

Other interpolation formulae for $n(\lambda)$ are given in [95Bac], [95Bas, Vol. II, Chap. 32], [05Gro1, p. 121].

Further information is available from glass catalogs (see Sect. 3.1.5.10) and from subroutines in commercial optical design programs:

- *relative dispersive power* or *Abbe's number* $\nu_d = \dfrac{n_d - 1}{n_F - n_C}$ with n_d(587.56 nm = yellow He-line), n_F(486.13 nm = blue H-line), n_C(656.27 nm = red H-line) [95Bac, 80Sch]; *application:* achromatic correction of systems [84Haf],
- spectral range of *transmission*,
- *temperature coefficients* of n and ν_d,
- *photoelastical coefficients*,
- *Faraday's effect* (Verdet's constant),
- chemical resistance, thermal conductivity, micro hardness etc.

Sellmeier-like formulae for crystals are available in [95Bas, Vol. II, Chap. 32]. Information in connection with laser irradiation damage is presented in [82Hac]. Specific values of *laser glasses* are given in tables in [01Iff].

3.1.5.3 Dispersion characteristics for short-pulse propagation

The parameters can be calculated from the dispersion interpolation (3.1.62) [91Sal, 96Die]:

$$\beta(\nu) = n(\nu)\,\frac{2\pi\,\nu}{c_0} \quad (\textit{propagation constant}\ [m^{-1}]) \,, \tag{3.1.63}$$

$$c_{ph} = \frac{c_0}{n(\nu)} \quad (\textit{phase velocity}\ [m\ s^{-1}]) \,, \tag{3.1.64}$$

$$v = \frac{2\pi}{\frac{\mathrm{d}\beta}{\mathrm{d}\nu}} = \frac{1}{\frac{\mathrm{d}\beta}{\mathrm{d}\omega}} \quad (\textit{group velocity } [\mathrm{m\ s^{-1}}]) \,, \tag{3.1.65}$$

$$D_v = \frac{1}{2\pi}\frac{\mathrm{d}^2\beta}{\mathrm{d}\nu^2} = 2\pi\frac{\mathrm{d}^2\beta}{\mathrm{d}\omega^2} = \frac{\mathrm{d}}{\mathrm{d}\nu}\left(\frac{1}{v}\right) \quad (\textit{group velocity dispersion } (GVD)) \tag{3.1.66}$$

with

ν : frequency of light,
c_0 : velocity of light in vacuum.

Application: Temporal pulse forming by the GVD of dispersive optical elements [96Die, 01Ben].

3.1.5.4 Optics of metals and semiconductors

The refractive index of *metals* is characterized by free-electron contributions ($\omega_0 = 0$ in (3.1.61)). One obtains from [67Sok, 72Woo], [95Bas, Vol. II, Chap. 35] with a plasma resonance (here collision-free: $\gamma = 0$):

$$n^2(\omega) = 1 - \left(\frac{\omega_\mathrm{p}}{\omega}\right)^2 \tag{3.1.67}$$

with

ω_p [$\mathrm{s^{-1}}$]: plasma frequency, depending on free-electron density [88Kle].

From (3.1.67) follows

- $n(\omega) < 1$ for $\omega > \omega_\mathrm{p}$, which means $\lambda < \lambda_\mathrm{p}$ (example: $\lambda_\mathrm{p} = 209$ nm for Na): transparency,
- pure imaginary $n(\omega)$ for $\omega < \omega_\mathrm{p}$, $\lambda_\mathrm{p} < \lambda$.

Other effects change the ideal case (3.1.67) [88Kle].

The complex refractive index of *semiconductors* is determined by transitions of electrons between or within the energy bands and by photon interaction with the crystal lattice (reststrahlen wavelength region). It depends strongly on the wavelength and is modified by heterostructures and dopands [71Pan, 95Kli], [95Bas, Vol. II, Chap. 36].

3.1.5.5 Fresnel's formulae

Fresnel's formulae describe the transmission and reflection of plane light waves at a plane interface between

- homogeneous isotropic media: [99Bor, 88Kle] and other textbooks on optics,
- homogeneous isotropic medium and anisotropic medium: special cases [99Bor, 86Haf] and other textbooks on optics,
- general case of anisotropic media: [58Fed],
- modification by photonic crystals: [95Joa, 01Sak].

Fresnel's formulae for the *amplitude* (field) *reflection and transmission coefficients* are listed in Table 3.1.7.

Plane of incidence: plane, containing the wave number vector $\boldsymbol{k}$ of the light and the normal vector $\boldsymbol{n}$ on the interface.

Table 3.1.7. Fresnel's formulae for the *amplitude* (field) *reflection and transmission coefficients.*

Case	The four values Θ, Θ', $\hat{n}$, and $\hat{n}'$ are considered	Using the angles Θ and Θ' only	sin Θ' is eliminated $\bar{n} = \frac{\hat{n}'}{\hat{n}}$	
Reflection				
$r_s = \frac{E_s''}{E_s} =$	$\frac{\hat{n}\ \cos\Theta - \hat{n}'\ \cos\Theta'}{\hat{n}\ \cos\Theta + \hat{n}'\ \cos\Theta'}$	$-\frac{\sin(\Theta - \Theta')}{\sin(\Theta + \Theta')}$	$\frac{\cos\Theta - \sqrt{\bar{n}^2 - \sin^2\Theta}}{\cos\Theta + \sqrt{\bar{n}^2 - \sin^2\Theta}}$	(3.1.68)
Reflection				
$r_p = \frac{E_p''}{E_p} =$	$\frac{\hat{n}'\ \cos\Theta - \hat{n}\ \cos\Theta'}{\hat{n}'\ \cos\Theta + \hat{n}\ \cos\Theta'}$	$\frac{\tan(\Theta - \Theta')}{\tan(\Theta + \Theta')}$	$\frac{\bar{n}^2\cos\Theta - \sqrt{\bar{n}^2 - \sin^2\Theta}}{\bar{n}^2\cos\Theta + \sqrt{\bar{n}^2 - \sin^2\Theta}}$	(3.1.69)
Transmission				
$t_s = \frac{E_s'}{E_s} =$	$\frac{2\hat{n}\ \cos\Theta}{\hat{n}'\ \cos\Theta + \hat{n}\ \cos\Theta'}$	$\frac{2\ \sin\Theta'\ \cos\Theta}{\sin(\Theta + \Theta')}$	$\frac{2\ \cos\Theta}{\cos\Theta + \sqrt{\bar{n}^2 - \sin^2\Theta}}$	(3.1.70)
Transmission				
$t_p = \frac{E_p'}{E_p} =$	$\frac{2\hat{n}\ \cos\Theta}{\hat{n}'\ \cos\Theta + \hat{n}\ \cos\Theta'}$	$\frac{2\ \sin\Theta'\ \cos\Theta}{\sin(\Theta + \Theta')\ \cos(\Theta - \Theta')}$	$\frac{2\bar{n}\ \cos\Theta}{\cos\Theta + \bar{n}^2\sqrt{\bar{n}^2 - \sin^2\Theta}}$	(3.1.71)
Application of cases	Mostly used for pure dielectric media.	In a stack of films, the angles to the axis were calculated previously.	See remark in Sect. 3.1.5.5.	

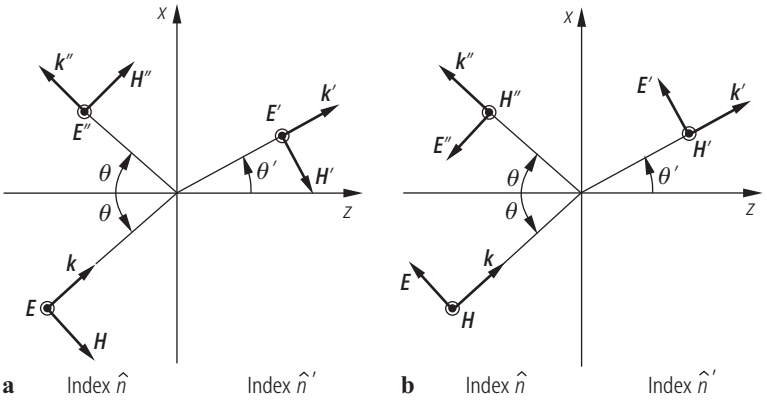

a **b**

Fig. 3.1.18. Refraction at an interface, represented in the plane of incidence: (**a**) E_s-case, (**b**) E_p-case. The commonly used *convention* is shown for the orientation of the relevant vectors ($\boldsymbol{k}$: the wave number vector, $\boldsymbol{E}$: the electrical field, and $\boldsymbol{H}$: the magnetic field) ensuring that $\boldsymbol{k}$, $\boldsymbol{E}$, and $\boldsymbol{H}$ are a right-handed system in every case. The $\boldsymbol{E}$-field is important for the action on a nonmagnetic material.

Polarization:

- $\boldsymbol{E}$ *perpendicular* to the plane of incidence: s-polarization (TE-case or σ-case [88Kle]), the corresponding $\boldsymbol{E}$-component is called $E_\perp$ [99Bor] or E_s (s: "senkrecht" (German) which means "perpendicular") [88Yeh] or index E [97Hua] or index x [90Roe, 77Azz, 91Sal].
- $\boldsymbol{E}$ *parallel* to the plane of incidence: p-polarization (TM-case or π-case [88Kle]), the corresponding $\boldsymbol{E}$-component is called $E_\parallel$ [99Bor] or E_p [88Yeh] or index M [97Hua] or index y [90Roe, 77Azz, 91Sal].

Snell's law:

$$\hat{n}\ \sin\Theta = \hat{n}'\ \sin\Theta' \tag{3.1.72}$$

with

$\hat{n}$, $\hat{n}'$: refractive indices of both media, respectively,
Θ, Θ': see Fig. 3.1.18.

Other convention than Fig. 3.1.18b [58Mac, 89Gha, 91Ish] (electrical engineering) on the orientation of the $\boldsymbol{E}$-vectors: $\boldsymbol{E}$ and $\boldsymbol{E}''$ point into the same direction for $\Theta \to 0$, $\boldsymbol{H}$ changes sign; application: $\boldsymbol{E}$-interferences.

Remark:

- $\hat{n}$ is real and $\hat{n}'$ is complex (*absorption* [76Fed, 77Azz] or *gain* [88Boi]).
- $\hat{n}$ and $\hat{n}'$ are real and $\bar{n} = \dfrac{\hat{n}'}{\hat{n}} < 1$ and $(\bar{n}^2 - \sin^2\Theta) < 0$ (*total reflection*). Then $\sqrt{\bar{n}^2 - \sin^2\Theta} = \mathrm{i}\sqrt{\sin^2\Theta - \bar{n}^2}$ yields for (3.1.68) and (3.1.69) $r_s = \exp(\mathrm{i}\,\delta_s)$ and $r_p = \exp(\mathrm{i}\,\delta_p)$ (modulus = 1, all energy reflected) and $\tan\dfrac{\delta_s}{2} = -\dfrac{\sqrt{\sin^2\Theta - \bar{n}^2}}{\cos\Theta}$ and $\tan\dfrac{\delta_p}{2} = -\dfrac{\sqrt{\sin^2\Theta - \bar{n}^2}}{\bar{n}^2\cos\Theta}$.

The intensities in the media are calculated with help of the z-component of Poynting's vector [88Kle, 90Roe, 76Fed].

Reflectance (reflected part of intensity):

$$R_{s,p} = |r_{s,p}|^2\ . \tag{3.1.73}$$

Transmittance (transmitted part of intensity):

$$T_{\mathrm{s,p}} = \frac{\mathrm{Re}\,(\hat{n}'\cos\Theta')}{\mathrm{Re}\,(\hat{n}\cos\Theta)}\ |t_{\mathrm{s,p}}|^2 \tag{3.1.74}$$

with

Re : real part.

Energy conservation:

$$T_{\mathrm{s,p}} + R_{\mathrm{s,p}} = 1\ .$$

3.1.5.6 Special cases of refraction

3.1.5.6.1 Two dielectric isotropic homogeneous media ($\hat{n}$ and $\hat{n}'$ are real)

$$r_{\mathrm{s}} = \frac{n - n'}{n + n'} = -r_{\mathrm{p}}\ . \tag{3.1.75}$$

(The negative sign of r_{p} results from the convention of Fig. 3.1.18 that E_{p} is diffracted into $-E_{\mathrm{p}}''$).

$$R_{\mathrm{s}} = R_{\mathrm{p}} = \left(\frac{n - n'}{n + n'}\right)^2 \quad \text{and} \quad T_{\mathrm{s}} = T_{\mathrm{p}} = 1 - R_{\mathrm{s}}\ . \tag{3.1.76}$$

Example 3.1.8. $n = 1$, $n' = 1.5$ (glass): $R_{\mathrm{s}} = 0.04$.

3.1.5.6.2 Variation of the angle of incidence

3.1.5.6.2.1 External reflection ($n < n'$)

Brewster's angle (angle of polarization) Θ_{B} :

$$\Theta_{\mathrm{B}} + \Theta'_{\mathrm{B}} = 90^\circ\ , \quad R_{\mathrm{p}} = 0\ , \quad \tan\Theta_{\mathrm{B}} = \frac{n'}{n}\ . \tag{3.1.77}$$

Example 3.1.9. $n = 1$, $n' = 1.5$, $\Theta_{\mathrm{B}} = 56.3^\circ$. See Fig. 3.1.19.

3.1.5.6.2.2 Internal reflection ($n > n'$)

Critical angle of total reflection:

$$\sin\Theta_{\mathrm{C}} = \frac{n'}{n}\ . \tag{3.1.78}$$

Total reflection: $\Theta > \Theta_{\mathrm{C}}$ with $|r_{\mathrm{s}}| = |r_{\mathrm{p}}| = 1$ and the phases of the reflected waves: $r_{\mathrm{s}} = \exp(\mathrm{i}\,\Phi_{\mathrm{s}})$ and $r_{\mathrm{p}} = \exp(\mathrm{i}\,\Phi_{\mathrm{p}})$.

Brewster's angle:

$$\tan\Theta_{\mathrm{B}} = \frac{n'}{n}\ . \tag{3.1.79}$$

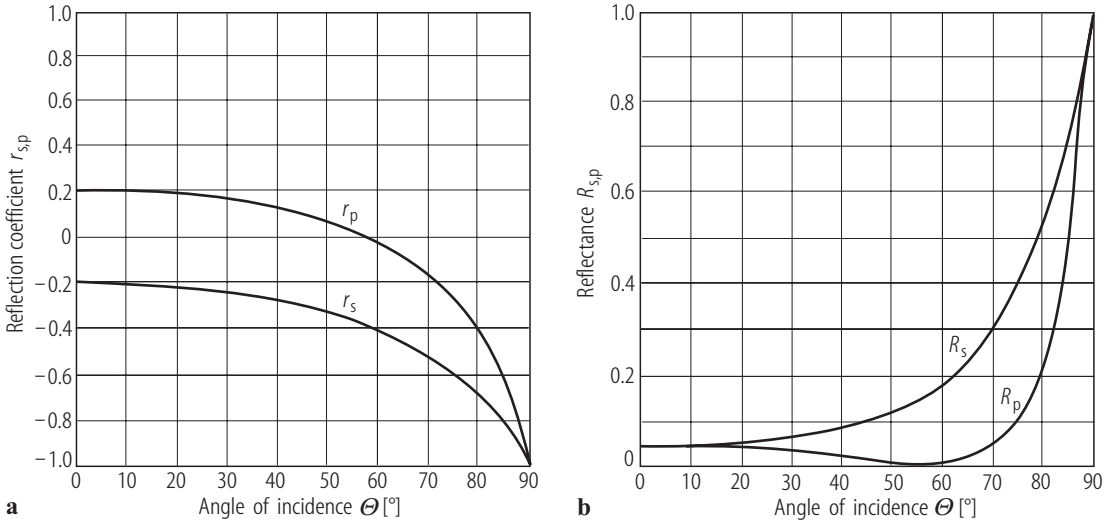

Fig. 3.1.19. (**a**) Reflection coefficients r_p and r_s and (**b**) reflectances R_p and R_s for $n = 1$ and $n' = 1.5$.

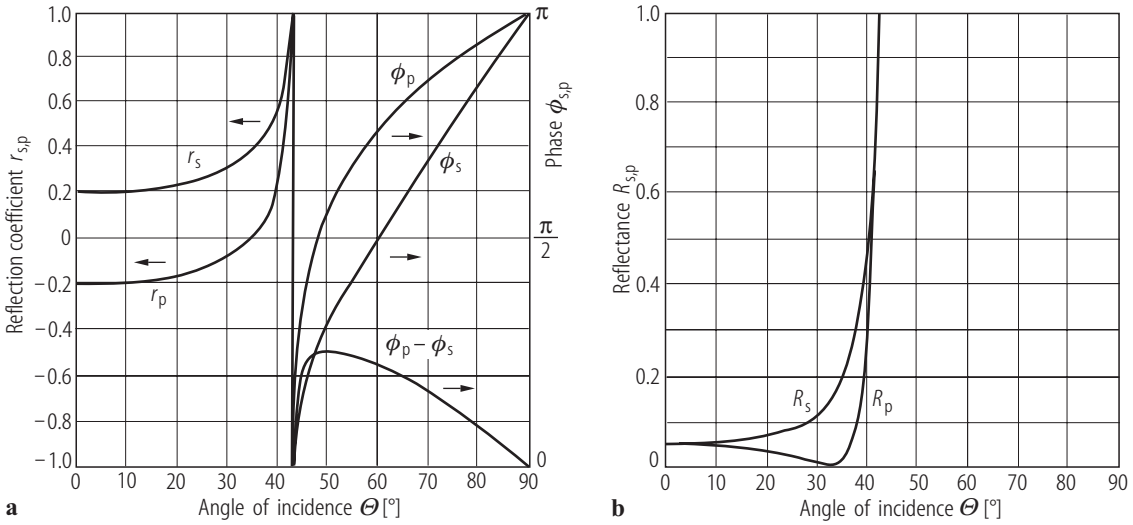

Fig. 3.1.20. Internal reflection ($n = 1.5$, $n' = 1$). (**a**) Reflection coefficients r_p and r_s for $\Theta < \Theta_C$ and phases Φ_p and Φ_s for $\Theta > \Theta_C$. (**b**) Reflectances R_p and R_s ($= 1$ for $\Theta > \Theta_C$).

Example 3.1.10. $n = 1.5$, $n' = 1$, $\Theta_C = 41.8°$, $\Theta_B = 33.7°$. See Fig. 3.1.20.

Penetration depth in Fig. 3.1.21 [88Kle, p. 67]:

$$d_{pen} = \frac{\lambda_0}{2\pi\sqrt{n^2 \sin^2\Theta - n'^2}} \,. \tag{3.1.80}$$

Goos–Hänchen shift [88Yeh, p. 74], see Fig. 3.1.22:

$$d_{G.-H.,s,p} = \frac{d\Phi_{s,p}}{d\Theta} \tag{3.1.81}$$

with Φ_p and Φ_s from Fig. 3.1.20. For a more precise treatment of the Goos–Hänchen shift for Gaussian beams see [05Gro1, p. 100].

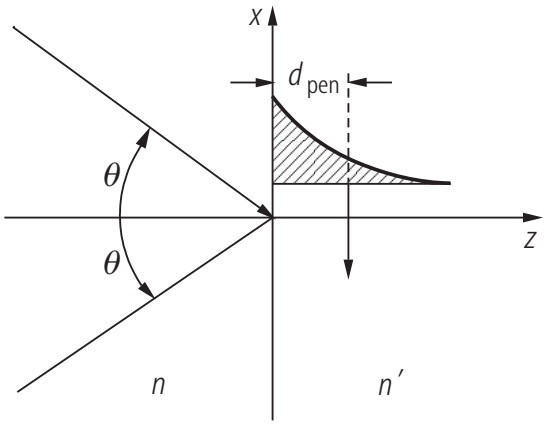

Fig. 3.1.21. Total reflection of plane waves with an inhomogeneous wave in the medium with the refractive index n' (d_{pen} : amplitude $\Rightarrow 1/e$).

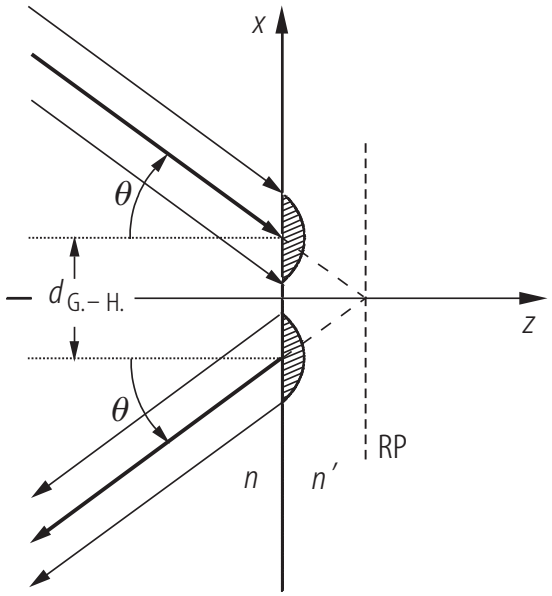

Fig. 3.1.22. Goos–Hänchen shift of a total reflected beam with finite (exaggerated small) cross section (RP: effective reflection plane).

3.1.5.6.3 Reflection at media with complex refractive index (Case $\hat{n} = 1$ and $\hat{n}' = n' + \mathrm{i}\,k'$)

In Fig. 3.1.23 the refractive index n and the attenuation index k of gold (Au) is shown, in Fig. 3.1.24 the reflectance for both polarization cases of gold is given.

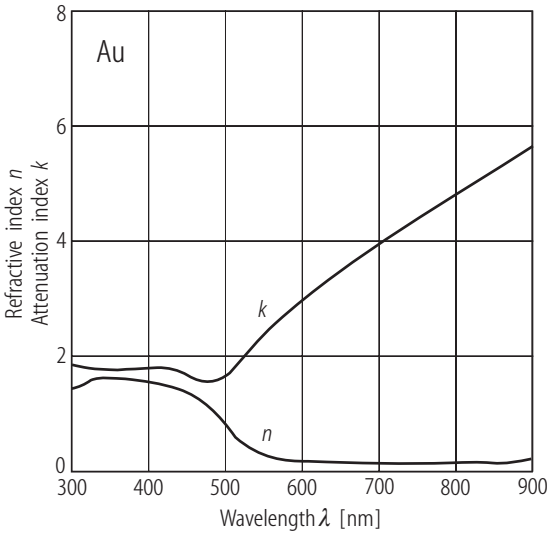

Fig. 3.1.23. Refractive index n and attenuation index k of gold (Au).

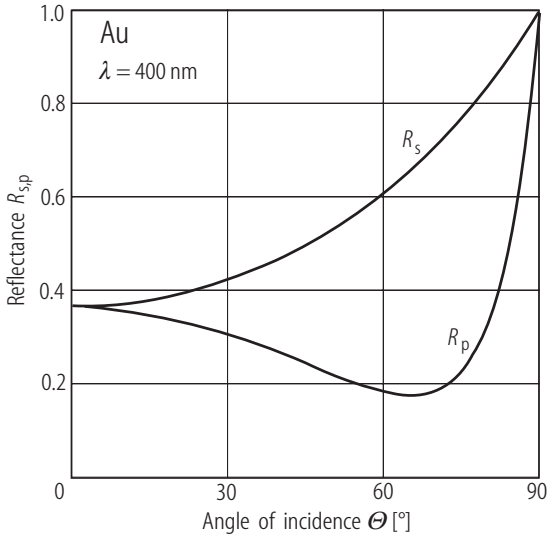

Fig. 3.1.24. Reflectance for both polarization cases of gold (Au). There is a minimum of R_p which is connected with a *pseudo Brewster angle*.

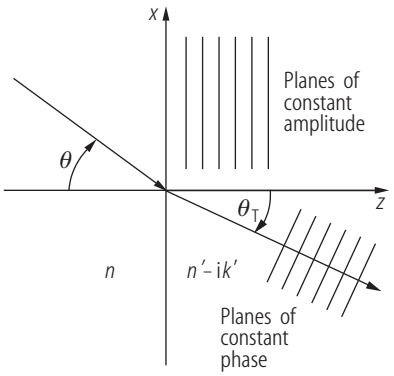

Fig. 3.1.25. Refraction at a medium with absorption: generation of an inhomogeneous wave.

Inhomogeneous wave (Fig. 3.1.25): *Snell's refraction law* is modified:

$$\sin \Theta_{\mathrm{T}} = \frac{n}{n_{\mathrm{T}}} \sin \Theta \tag{3.1.82}$$

with

$$2\,n_{\mathrm{T}}^2 = n'^2 - k'^2 + n^2 \sin^2 \Theta + \sqrt{\left(n'^2 - k'^2 - n^2 \sin^2 \Theta\right)^2 + 4\,n'^2\,k'^2} \quad \text{(Ketteler's formula)} .$$

The effective refractive index n_{T} determines the direction angle Θ_{T} of planes of constant phase in Fig. 3.1.25 via (3.1.82) [88Kle, p. 78], [41Str, p. 503], [99Bor, p. 740]. The full inhomogeneous wave can be calculated using [99Bor, p. 740].

Example 3.1.11. $\Theta = 45\,^\circ$, Au: $\lambda = 800$ nm, $n' = 0.19$, $k' = 4.9$, $n_{\mathrm{T}} = 0.73$, $\Theta_{\mathrm{T}} = 75.1\,^\circ$ (see [28Koe, p. 209]).

Intensity attenuation in the case $\Theta = 0\,^\circ$:

$$I = I_0 \exp\left\{-2\,(\omega/c)\,k'\,z\right\} . \tag{3.1.83}$$

Example 3.1.12. $\Theta = 0\,^\circ$, Au: $\lambda = 800$ nm, $n' = 0.19$, $k' = 4.9$, $I = I_0 \exp\left(-7.7 \times 10^4\, z[\mathrm{mm}]\right)$, $1/\mathrm{e} - \mathrm{depth} = 13$ nm.

Ellipsometry: $\delta_{\mathrm{p}} - \delta_{\mathrm{s}}$ and moduli $\dfrac{|r_{\mathrm{p}}|}{|r_{\mathrm{s}}|}$ of the reflected light $r_{\mathrm{p}} = |r_{\mathrm{p}}| \exp\left(\mathrm{i}\,\delta_{\mathrm{p}}\right)$ and $r_{\mathrm{s}} = |r_{\mathrm{s}}| \exp\left(\mathrm{i}\,\delta_{\mathrm{s}}\right)$ can be measured. The complex refractive index of a material results [77Azz, 90Roe]. Application: Measurements for the optical constants of metals, semiconductors, and thin-film systems.

3.1.5.7 Crystal optics

3.1.5.7.1 Classification

The dielectric tensor $\varepsilon_{\mathrm{r}} = \varepsilon_{ij}$ in (1.1.8) is symmetrical and real in the case of a nonabsorbing medium.

In Fig. 3.1.26 vectors connected with wave propagation in crystal optics are depicted. In Table 3.1.8 optical crystals are listed. In Table 3.1.9 three of the eight surfaces for visualization of wave propagation in crystals are presented.

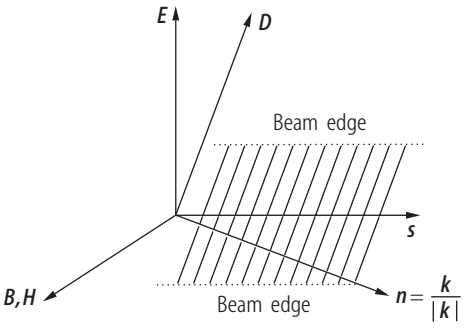

Fig. 3.1.26. Vectors connected with wave propagation in crystal optics [99Bor]: $\boldsymbol{s}$: ray direction unit vector ∥ Poynting vector $\boldsymbol{E} \times \boldsymbol{H}$, $\boldsymbol{n}$: unit vector in the normal direction ∥ $\boldsymbol{k}$ and ⊥ phase planes, orthogonalities: $\boldsymbol{B}, \boldsymbol{H} \perp \boldsymbol{E}, \boldsymbol{D}, \boldsymbol{n}, \boldsymbol{s}$; $\boldsymbol{E} \perp \boldsymbol{s}$; $\boldsymbol{D} \perp \boldsymbol{n}$.

Table 3.1.8. Optical crystals.

Classification: system (syngony) of crystal	Refractive index in the main axis system	Optical type of crystal	Example	Values of the refractive index for $\lambda = 589.3$ nm
triclinic, monoclinic, orthorhombic	$n_x \neq n_y \neq n_z \neq n_x$	biaxial crystal, no ordinary waves	$NaNO_3$	$n_x = 1.344$, $n_y = 1.411$, $n_z = 1.651$
trigonal, tetragonal, hexagonal	$n_x = n_y = n_o$ (ordinary index)	positive uniaxial crystal: $n_o < n_e$	SiO_2 (quartz)	$n_o = 1.544$, $n_e = 1.553$
	$n_x \neq n_z = n_e$ (extraordinary index)	negative uniaxial crystal: $n_o > n_e$	$CaCO_3$ (calcite)	$n_o = 1.658$, $n_e = 1.486$
cubic	$n_x = n_y = n_z = n$	isotropic crystal	NaCl	$n = 1.544$

Table 3.1.9. Three of the eight surfaces for visualization of wave propagation in crystals.

Surface	Given	Found by construction are the
Index ellipsoid (indicatrix) (one-shell surface)	normal direction $\boldsymbol{n}$	$\boldsymbol{D}$-vectors for the two polarization cases and the two refractive indices for phase propagation
Index surface, wave vector surface (two-shell surface)	normal direction $\boldsymbol{n}$	ray directions $\boldsymbol{s}$, which are perpendicular to the surface for both polarization cases
Ray surface, wave surface, representing Huygens' elementary wave for both polarization cases (two-shell surface)	ray direction $\boldsymbol{s}$	normal direction $\boldsymbol{n}$, which is perpendicular to the surface

Main feature of *crystal optics*: $\boldsymbol{s}$ *is not parallel with* $\boldsymbol{n}$ for wave propagation, mostly.

- $\boldsymbol{s}$ is essential for description of the energy propagation (edges of bundles, rays),
- $\boldsymbol{n}$ is essential for description of the interferences of infinite broad waves.

References: [28Szi, 54Bel, 58Shu, 61Ram, 76Fed, 79Wah, 84Yar, 04Ber, 99Pau, 99Bor]. A detailed comparison between that surfaces is given in [28Szi].

3.1.5.7.2 Birefringence (example: uniaxial crystals)

Uniaxial crystals in the plane of incidence:

– *Refraction of the normal direction* $\boldsymbol{n}$ of wavefronts: The wavevector surface is shown in Fig. 3.1.27.

$$\sin\Theta_\mathrm{o} = \frac{n}{n_\mathrm{o}} \sin\Theta \quad (\textit{ordinary wave } (\boldsymbol{k}_\mathrm{o})) \tag{3.1.84}$$

(n_o *does not depend* on the angle of incidence),

$$\sin\Theta_\mathrm{e} = \frac{n}{n_{\theta\,\mathrm{e}}\,(\Theta_\mathrm{e}(\Theta))} \sin\Theta \quad (\textit{extraordinary wave } (\boldsymbol{k}_\mathrm{e})) \tag{3.1.85}$$

(n_e *depends* on the angle of incidence).

– *Refraction of rays* (Poynting vector): $\boldsymbol{s}_\mathrm{e}$ and $\boldsymbol{s}_\mathrm{o}$ are given by tangent construction in Fig. 3.1.28.

– *Algorithm* for the calculation of $\boldsymbol{k}_\mathrm{o}$ ($\|\boldsymbol{s}_\mathrm{o}$), $\boldsymbol{k}_\mathrm{e}$, $\boldsymbol{s}_\mathrm{e}$ of Fig. 3.1.28 with n, n_o, n_e, η, θ of Fig. 3.1.29 [86Haf]:

$$n_{\theta\,\mathrm{e}}^2 = \frac{A}{B} + \frac{n^2(n_\mathrm{o}^2 - n_\mathrm{e}^2)^2 \sin^2\Theta \sin^2(2\eta)}{2\,B^2} \pm \frac{n(n_\mathrm{o}^2 - n_\mathrm{e}^2)^2 \sin\Theta \sin(2\eta)}{B} \times \sqrt{n^2 \sin^2\Theta \left[\frac{(n_\mathrm{o}^2 - n_\mathrm{e}^2)^2 \sin^2(2\eta)}{4B^2} - 1\right] + \frac{A}{B}} \tag{3.1.86}$$

(*refractive index for the extraordinary wave*)

with

$$A = (n_\mathrm{e}^2 - n_\mathrm{o}^2)\, n^2 \sin^2\Theta \cos(2\eta) - n_\mathrm{o}^2\, n_\mathrm{e}^2 \,,$$

$$B = n_\mathrm{o}^2 + (n_\mathrm{e}^2 - n_\mathrm{o}^2) \sin^2\eta \,,$$

where the decision on the ± sign in (3.1.86) can be made by controlling the satisfaction of

$$n_{\theta\,\mathrm{e}}^2 \left[n_\mathrm{o}^2 + (n_\mathrm{e}^2 - n_\mathrm{o}^2) \sin^2(\eta + \Theta_\mathrm{e})\right] = n_\mathrm{e}^2\, n_\mathrm{o}^2 \,.$$

The resulting angles are:

$$\Theta_\mathrm{o} = \arcsin(n \sin\Theta / n_\mathrm{o}) \,, \tag{3.1.87}$$

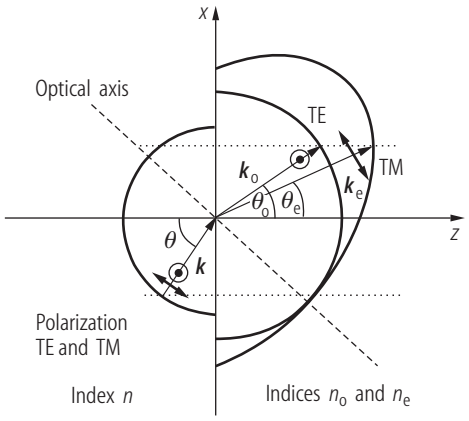

Fig. 3.1.27. Construction of wavefront birefringence with the wavevector surface: The wavefronts show no transversal limitation.

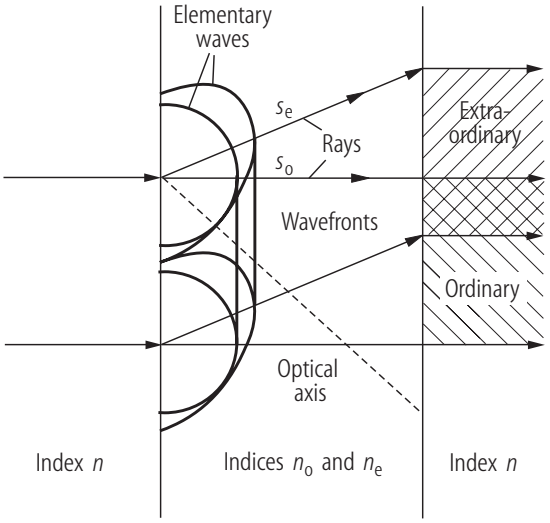

Fig. 3.1.28. Huygens' tangent construction of birefringence in a crystal slab for transversal-limited beams.

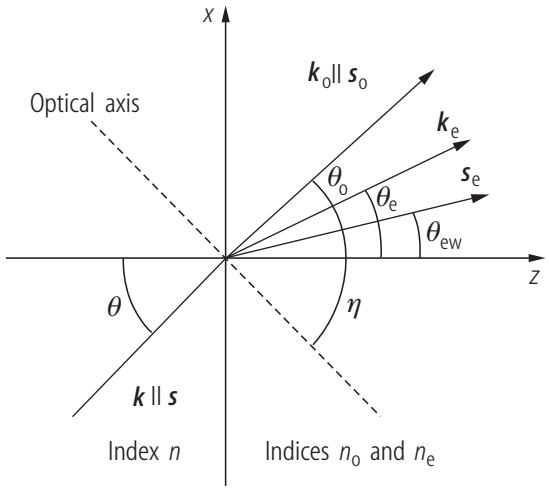

Fig. 3.1.29. Refraction for normal and ray directions. η: angle between z-axis and optical axis.

$$\Theta_e = \arcsin\left(n \sin\Theta / n_{\Theta e}\right) , \tag{3.1.88}$$

$$\Theta_{ew} = \arctan \frac{\tan\eta - C}{1 + C \tan\eta} \tag{3.1.89}$$

with

$$C = \frac{n_o^2}{n_e^2} \times \frac{\sqrt{n_{\Theta e}^2 - n^2 \sin^2\Theta}\ \tan\eta + n \sin\Theta}{\sqrt{n_{\Theta e}^2 - n^2 \sin^2\Theta}\ - n \sin\Theta \tan\eta} .$$

Application: Θ_e, Θ_o, n_o, and $n_{\Theta e} \Rightarrow$ phase differences (interferences) and reflection coefficient, Θ_o and $\Theta_{ew} \Rightarrow$ ray separation in a crystal.

Example 3.1.13. Calcite: $n_o = 1.658$, $n_e = 1.486$, $\eta = 45°$: #1: $\Theta = 0°$: $C = 1.244822$, $n_{\Theta e} = 1.565$, $\Theta_o = \Theta_e = 0°$, $\Theta_{ew} = -6.224°$; #2: $\Theta = 45°$: $n_{\Theta e} = 1.636$, $C = 0.438329$, $\Theta_o = 25.23°$, $\Theta_e = 25.6°$, $\Theta_{ew} = 21.33°$.

General formulation of (3.1.85)–(3.1.89): see [76Fed, Table 9.1] for more detailed discussions.

3.1.5.8 Photonic crystals

Starting with the forbidden (stop) bands in case of multi-layer Bragg reflection [88Yeh, p. 123] a material class is under development which stops light propagation along as many directions and for as many wavelengths as possible. This suppresses the spontaneous emission for laser applications and opens new possibilities in the micro- and nano-optics [95Joa, 01Sak, 04Bus]. Photonic crystal fibers [04Bus] can be designed for special light propagation properties and high-power fiber lasers [03Wad].

3.1.5.9 Negative-refractive-index materials

The common excitation of electrical dipoles and magnetical dipoles by light in a medium can result in a negative dielectric permittivity $\mathrm{Re}\,(\varepsilon) < 0$ in combination with a negative magnetic permeability $\mathrm{Re}\,(\mu) < 0$. Then, in Snell's law (3.1.72) an effective index $\hat{n}\,' < 0$ is possible [68Ves] which results in imaging by a slab of this material without curved surfaces [00Pen] and other interesting effects [05Ram]. Such metamaterials can be generated by microtechnology, now for mm- and terahertz-waves, but with the trend towards visible radiation [05Ele].

3.1.5.10 References to data of linear optics

[62Lan] contains optical constants, only. In later editions, the optical constants are listed together with other properties of substances. An overview is given in the content volume [96Lan].

Optical glass:	[62Lan, Chap. 283], [97Nik], [95Bas, Vol. 2, Chap. 33], catalogs of producers: [96Sch, 98Hoy, 96Oha, 92Cor], and commercial optical design programs.
Infrared materials:	[98Pal, 91Klo], [96Sch, infrared glasses], commercial optical design programs.
Crystals:	[62Lan, Chap. 282], [95Bas, Vol. 2, Chap. 33], [97Nik, 91Dmi, 81Kam].
Photonic crystals:	[95Joa, 01Sak, 04Bus].
Negative-refractive-index materials:	[05Ram].
Polymeric materials:	[62Lan, Chap. 283], [95Bas, Vol. 2, Chap. 34], [97Nik].
Metals:	[62Lan, Chap. 281], [98Pal], [95Bas, Vol. 2, Chap. 35].
Semiconductors:	[96Lan, 98Pal, 87EMI], [95Bas, Vol. 2, Chap. 36].
Solid state laser materials:	[01Iff, 97Nik, 81Kam].
Liquids:	[62Lan, Chaps. 284, 285], [97Nik].
Gases:	[62Lan, Chap. 286].

3.1.6 Geometrical optics

Geometrical optics represents the limit of the wave optics for $\lambda \Rightarrow 0$.

The development $\sin\sigma = \sigma - \frac{1}{3!}\sigma^3 + \frac{1}{5!}\sigma^5 - \ldots$ with σ the angle in Snell's law characterizes the different approaches of geometrical optics. Table 3.1.10 gives an overview of different approximations of geometrical optics.

3.1.6.1 Gaussian imaging (paraxial range)

The signs of the parameters determined in [03DIN, 96Ped] are applied in Sect. 3.1.6.1.1, later on $f = f'$ is used.

Table 3.1.10. Different approximations of geometrical optics.

Problem to be treated	Algorithm for solving
Given: object point O in the paraxial range, *asked*: image point O' in the *paraxial range* approximation: $\sin\sigma \approx \sigma$.	– Gaussian collineation and Listing's construction: see Sect. 3.1.6.1. – Gaussian matrix formalism (ABCD-matrix): see Sect. 3.1.6.2, ref.: [04Ber, 99Bor].
Imaging in *Seidel's range*, *asked*: imaging quality approximation: $\sin\sigma \approx \sigma - \frac{1}{3!}\sigma^3$.	Formulae for Seidels aberrations: see Sect. 3.1.6.3, ref.: [70Ber, 80Hof, 84Haf, 84Rus, 86Haf, 91Mah].
General image formation.	(Commercial) raytracing programs with geometric and wave optical merit functions and tolerancing, ref.: [84Haf, 86Haf].

3.1.6.1.1 Single spherical interface

Figure 3.1.30 shows the imaging by a spherical interface in the paraxial range (small x, x', h).

Gaussian imaging equation:

$$n\left(\frac{1}{r}-\frac{1}{s}\right) = n'\left(\frac{1}{r}-\frac{1}{s'}\right) \quad \text{or} \quad \frac{n'}{s'} = \frac{n}{s} + \frac{n'-n}{r} \; . \tag{3.1.90}$$

Abbe's invariant $n\left(\frac{1}{r}-\frac{1}{s}\right)$ is a constant on both sides of the interface.

Object-space focal length:

$$f = -\frac{nr}{n'-n} \; . \tag{3.1.91}$$

Image-side focal length:

$$f' = \frac{n'r}{n'-n} \; . \tag{3.1.92}$$

Remark: The symbol f means outside this section, Sect. 3.1.6.1, the positive focal length for a positive (converging) lens.

Newton's imaging equation:

$$z\,z' = f\,f' \; . \tag{3.1.93}$$

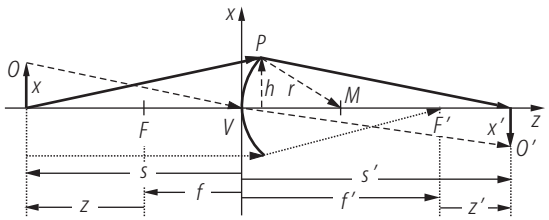

Fig. 3.1.30. Imaging by a spherical interface in the paraxial range (small x [object height], x' [image height], h [zonal height]). Full line: axial imaging, dashed line: off-axis imaging, dotted line: focusing to image side F'. *Sign conventions*: $s, s' > 0$, if they point to the right-hand side of the vertex V, $r > 0$, if the center of curvature of the interface is on the right-hand side in comparison with V. Here: $s < 0$, $s' > 0$, $r > 0$. M: center of curvature of the sphere. The left-hand-side-directed arrows symbolize negative values for the corresponding parameters here.

Lagrange's invariant:

$$x' n' s' = x n s \tag{3.1.94}$$

with

n: object-space refractive index,
n': image-space refractive index,
s: object distance,
s': image distance,
r: radius of curvature of the interface,
x: height of the object point,
x': height of the image point,
z: focus-related object distance,
z': focus-related image distance.

Imaging through an optical system: concatenation of the imaging of the spherical surfaces in succession via (3.1.90) by using $s_{\text{following surface}} = s'_{\text{prior surface}} - d$, d: the distance between the surfaces, and (3.1.94) for an object height $x \neq 0$.

3.1.6.1.2 Imaging with a thick lens

Figure 3.1.31 shows the axial imaging with a thick lens, Fig. 3.1.32 depicts *Listing's construction* for thick-lens imaging of a finite-height object point O to image point O'.

Thick-lens imaging equation:

$$-\frac{1}{a} + \frac{1}{a'} = \frac{1}{f'} = (n'-1)\left(\frac{1}{r_1} - \frac{1}{r_2}\right) + \frac{t\,(n'-1)^2}{n' r_1 r_2}\,. \tag{3.1.95}$$

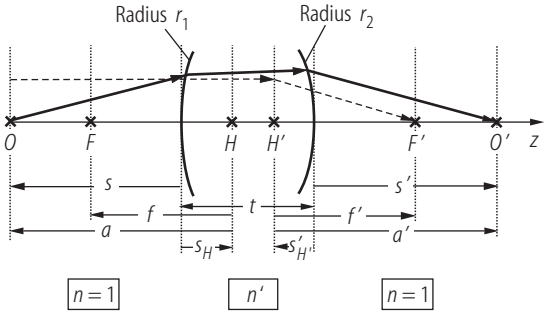

Fig. 3.1.31. Axial imaging with a thick lens. *Cardinal planes and points* are: *object-space principal plane* with object principal point H on axis, *image-space principal plane* with image principal point H' on axis, *object-space focal point* F, *image-space focal point* F'. *Nodal points* [98Mah, 96Ped] are equal to the principal points if O and O' are embedded in media with equal refractive index as here. Then $f = -f'$. The *sign convention* used here means: Parameters characterized by an arrow pointing to the left (right) hand side show a negative (positive) sign [80Hof, 86Haf]. The dashed line shows the use of H' for simplifying the plot for a ray focusing.

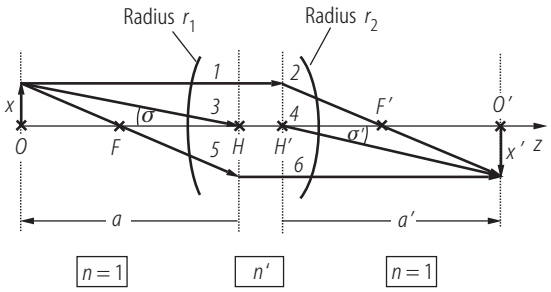

Fig. 3.1.32. *Listing's construction* for thick-lens imaging of a finite-height object point O to image point O'. Scheme of construction: Ray 1 (parallel with axis) is sharply bent at plane H' towards F'. Ray 3 towards H is continued at H' with the angle $\sigma' = \sigma$. Ray 5 through F is bent sharply parallel with axis at H-plane. The magnification $x'/x = a'/a$ can be calculated by elimination of a' from (3.1.95) $\Rightarrow x'$.

Position of the principal point H:

$$s_H = -\frac{n'-1}{n' r_2} f' t \,. \tag{3.1.96}$$

Position of the principal point H':

$$s_{H'} = -\frac{n'-1}{n' r_1} f' t \,. \tag{3.1.97}$$

Distance between the principal planes:

$$\overline{H\,H'} = t\left(1 - f'\,\frac{n'-1}{n'}\,\left(\frac{1}{r_1} - \frac{1}{r_2}\right)\right) \,. \tag{3.1.98}$$

Thin lens: $t \Rightarrow 0$: (3.1.95) $\Rightarrow$ "Lens maker's formula".

3.1.6.2 Gaussian matrix (ABCD-matrix, ray-transfer matrix) formalism for paraxial optics

Three tasks can be treated with the help of the ray-transfer matrix:

1. full description of *paraxial optics* (this section, Sect. 3.1.6.2),
2. *Gaussian beam propagation (coherent radiation)* by combination with a special beam calculation algorithm (see Sect. 3.1.7 on beam propagation),
3. *propagation of the second-order moments of the radiation field (inclusion of partial coherent radiation)* (see Chap. 2.2 on beam characterization).

The optical system can be the separating distance in an optical medium, a single spherical optical surface or a true, more complicated optical system.

There are *different definitions* for the ABCD-matrices:

Here: The slope components of the input and output rays are the real angles without any relation to the refractive indices at input and output spaces of Fig. 3.1.33 [66Kog1, 66Kog2, 84Hau, 91Sal, 95Bas, 96Ped, 96Yar, 98Hec, 98Sve, 01Iff, 05Gro1, 05Hod]. Then, the determinant of the matrix M: $\|\mathsf{M}\| = n'/n$ with n the index of the medium of the input plane and n' the index of the medium of the output plane.

Other authors [75Ger, 86Sie, 88Kle, 04Ber] use:
slope parameter = (angle) × (related refractive index). Then the equation $\|\mathsf{M}\| = 1$ applies.

In Fig. 3.1.34 the concatenation of different ray-transfer matrices for different types of subsystems is shown.

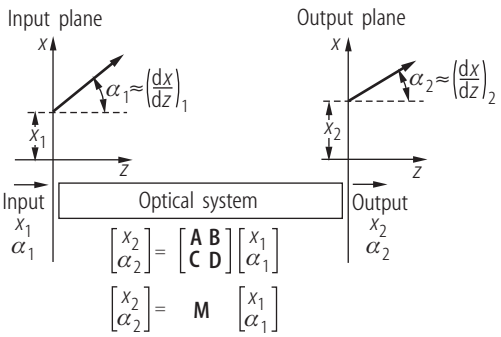

Fig. 3.1.33. Transfer of the input height x_1 and slope α_1 into the output height x_2 and slope α_2 with the ray-transfer matrix M. The *sign* of slope α_1 is positive in this figure. The German standard DIN 1335 uses a different sign with *change of some signs in the* ABCD *matrices* [96Ped].

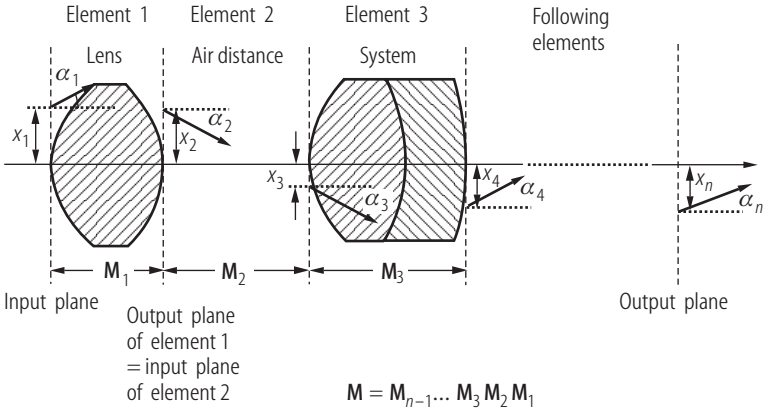

Fig. 3.1.34. Concatenation of different ray-transfer matrices for different types of sub-systems. Matrices known for systems before can be used to construct the matrix for a larger system containing the known systems. The sequence of the matrices is shown at the bottom of the figure.

3.1.6.2.1 Simple interfaces and optical elements with rotational symmetry

In Table 3.1.11 ABCD-matrices for simple interfaces and optical elements with rotational symmetry are listed.

3.1.6.2.2 Non-symmetrical optical systems

Rotational symmetry lacks and the axis is tilted due to the *non-symmetrical optical system*. In such a system, the central ray of imaging is called the basic ray. The optics in a narrow region around the basic ray is called *parabasal optics* [95Bas, Vol. 1, p. 1.47] as analogon to paraxial optics. For treatment of astigmatic pencils see [72Sta].

A special case of the non-symmetrical optical system is a *system without torsion*: Two orthogonal cases do not mix during propagation. Examples are different setups of spectroscopy and laser physics (ring resonators).

In Table 3.1.12 ABCD-matrices for non-symmetrical optical elements without torsion are listed.

3.1.6.2.3 Properties of a system

Properties of a system included in its ABCD-matrix are discussed in [75Ger, 96Ped, 05Hod, 05Gro1].

In Table 3.1.13 distances between *cardinal elements* of an optical system are listed, in Table 3.1.14 the meaning of the vanishing of different elements of the ABCD-matrix is depicted.

3.1.6.2.4 General parabolic systems without rotational symmetry

The generalization of the two-dimensional ray transfer after Fig. 3.1.33 to three dimensions [69Arn] is shown in Fig. 3.1.35. The ray in the input plane is characterized by two coordinates x_1 and y_1 of the piercing point P and two small (paraxial range) angles α_1 and β_1 .

The matrix S relates these parameters to the corresponding parameters in the output plane like in Fig. 3.1.33:

Table 3.1.11. ABCD-matrices for simple interfaces and optical elements with rotational symmetry.

Effect	Figure	ABCD-matrix	Remark
Propagation	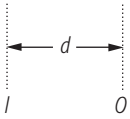	$\begin{bmatrix} 1 & d \\ 0 & 1 \end{bmatrix}$	The rays propagate from I to O within the same medium.
Spherical surface	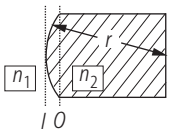	$\begin{bmatrix} 1 & 0 \\ \frac{n_1 - n_2}{n_2 r} & \frac{n_1}{n_2} \end{bmatrix}$	Sign: $r > 0$ for convex surface seen by the propagating light.
Plane	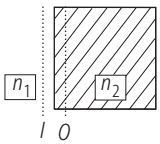	$\begin{bmatrix} 1 & 0 \\ 0 & \frac{n_1}{n_2} \end{bmatrix}$	Corresponds to a spherical surface with $r \Rightarrow \infty$.
Planar plate	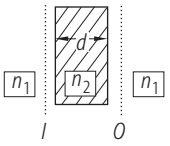	$\begin{bmatrix} 1 & \frac{n_1}{n_2} d \\ 0 & 1 \end{bmatrix}$	Contains two refractions.
Thin lens	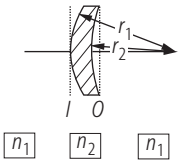	$\begin{bmatrix} 1 & 0 \\ -\frac{1}{f} & 1 \end{bmatrix}$	$\frac{1}{f} = \frac{n_2 - n_1}{n_1} \left[\frac{1}{r_1} - \frac{1}{r_2} \right]$, air: $n_1 = 1$.
Thick lens in air	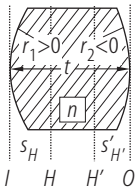	$\begin{bmatrix} 1 - \frac{s_{H'}}{f} & \frac{d}{n} \\ -\frac{1}{f} & 1 + \frac{s_H}{f} \end{bmatrix}$	$\frac{1}{f} = (n-1) \left[\frac{1}{r_1} - \frac{1}{r_2} \right] + \frac{(n-1)^2 t}{n r_1 r_2}$, $s_H = -\frac{(n-1) f t}{n r_2}$, see (3.1.96), $s_{H'} = -\frac{(n-1) f t}{n r_1}$, see (3.1.97), H, H': principal planes.
Spherical mirror	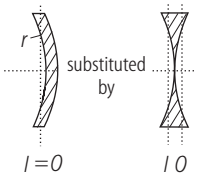	$\begin{bmatrix} 1 & 0 \\ -\frac{2}{r} & 1 \end{bmatrix}$	Unfolding of the mirror; sign$(r) > 0$, if the incident light sees a concave mirror surface.
Gradient-index lens or thermal lens	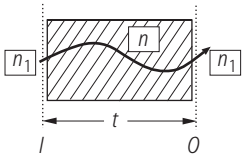	$\begin{bmatrix} A & B \\ C & D \end{bmatrix}$ $n = n_0 (1 - \gamma x^2)$; $\gamma > 0$: higher index on axis	$A = \cos\left(\sqrt{2\gamma}\, t\right)$; $B = n_1 \sin\left(\sqrt{2\gamma}\, t\right) / \left(n_0 \sqrt{2\gamma}\right)$; $C = -\left(\sqrt{2\gamma}\, n_0/n_1\right) \sin\left(\sqrt{2\gamma}\, t\right)$; $D = \cos\left(\sqrt{2\gamma}\, t\right)$; development of the trigonometric functions for $\sqrt{2\gamma}\, t \ll 1 \Rightarrow$ simplifications Gradient optics: see [02Gom, 05Gro1].

(continued)

Table 3.1.11 continued.

Effect	Figure	ABCD-matrix	Remark
Gaussian apodization, usable for q-parameter transfer (Table 3.1.18)	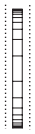	$\begin{bmatrix} 1 & 0 \\ -\frac{\mathrm{i}\,\lambda\,a}{2\,\pi} & 1 \end{bmatrix}$ λ: wavelength of light	The amplitude transmission function between I and O is $\exp\left(-a\,x^2/2\right)$, x: transverse coordinate [86Sie, p. 787]

Remark: Other treatments of the mirror see [86Sie, 98Sve, 75Ger].

Table 3.1.12. ABCD-matrices for non-symmetrical optical elements without torsion.

Effect	Figure	ABCD-matrix	Remark
Refraction at a sphere Tangential (meridional) plane	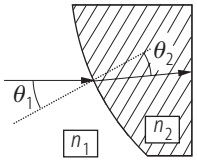	$\begin{bmatrix} \frac{\cos(\theta_1)}{\cos(\theta_2)} & 0 \\ \frac{\Delta\, n_\mathrm{t}}{r\, n_2} & \frac{n_1 \cos(\theta_2)}{n_2 \cos(\theta_1)} \end{bmatrix}$	$n_1\ \sin(\theta_1) = n_2\ \sin(\theta_2)$ (Snell's law) $\Delta\, n_\mathrm{t} = \frac{n_2\ \cos(\theta_2) - n_1\ \cos(\theta_1)}{\cos(\theta_1)\ \cos(\theta_2)}$
Sagittal plane	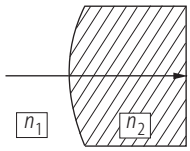	$\begin{bmatrix} 1 & 0 \\ \frac{\Delta\, n_\mathrm{s}}{r\, n_2} & \frac{n_1}{n_2} \end{bmatrix}$	$\Delta\, n_\mathrm{s} = n_2\ \cos(\theta_2) - n_1\ \cos(\theta_1)$
Rowland concave grating (unfolded) Tangential (meridional) plane	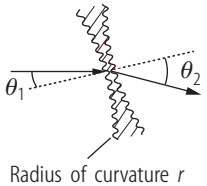	$\begin{bmatrix} A & B \\ C & D \end{bmatrix}$, $A = \frac{\cos(\theta_1)}{\cos(\theta_2)}$; $B = 0$; $C = -\frac{2\ \cos(\theta_2)}{r_\mathrm{t} \cos(\theta_1)}$; $D = A$.	Grating equation (3.1.52): $\sin(\theta_1) + \sin(\theta_2) = m\,\frac{\lambda}{g}$, $r_\mathrm{t} = \frac{2\,r\ \cos^2(\theta_2)}{\cos(\theta_1) + \cos(\theta_2)}$
Sagittal plane	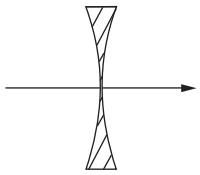	$\begin{bmatrix} 1 & 0 \\ -\frac{2}{r_\mathrm{s}} & 1 \end{bmatrix}$	$r_\mathrm{s} = \frac{2\,r}{\cos(\theta_1) + \cos(\theta_2)}$, general corrected holographical gratings: see [81Gue]
Spherical concave mirror		Specialization of the Rowland grating to $g \Rightarrow \infty$, $\theta_1 = \theta_2$.	

Table 3.1.13. Distances between *cardinal elements* of an optical system: F, F': object- and image-space focal points, respectively; H, H': object- and image-space principal points, respectively; I, O: input and output plane, respectively. The order of points determines the signs.

Distance between two points	A, B, C, and D for $n_1 = n_2$
$\overline{I\,F}$	$\frac{D}{C}$
$\overline{F\,H}$	$-\frac{1}{C}$
$\overline{O\,F'}$	$-\frac{A}{C}$
$\overline{H\,F'}$	$-\frac{1}{C}$

Table 3.1.14. The meaning of the vanishing of different elements of the ABCD-matrix.

Element	Figure	Remark
$A = 0$	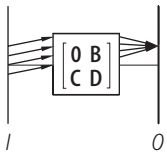	$x_2 = B\,\alpha_1$ *Focusing* of collimated light into the image-side focal plane.
$B = 0$	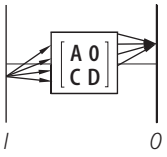	$x_2 = A\,x_1$ The input plane is *imaged* to the output plane (conjugated planes). A: magnification of imaging; appl.: calculation of image plane.
$C = 0$	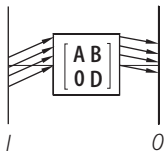	$\alpha_2 = D\,\alpha_1$ Transformation of collimated light into collimated light. D: angular magnification; *telescope* (*afocal* system).
$D = 0$	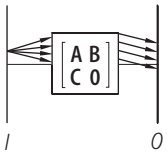	$\alpha_2 = C\,x_1$ *Collimation* of divergent pencil of rays. C: *power* of the element or system.

$$\begin{bmatrix} x_2 \\ y_2 \\ \alpha_2 \\ \beta_2 \end{bmatrix} = \begin{bmatrix} A_{xx} & A_{xy} & B_{xx} & B_{xy} \\ A_{yx} & A_{yy} & B_{yx} & B_{yy} \\ C_{xx} & C_{xy} & D_{xx} & D_{xy} \\ C_{yx} & C_{yy} & D_{yx} & D_{yy} \end{bmatrix} \begin{bmatrix} x_1 \\ y_1 \\ \alpha_1 \\ \beta_1 \end{bmatrix} \quad \text{or} \quad \begin{bmatrix} \boldsymbol{r}_2 \\ \boldsymbol{\gamma}_2 \end{bmatrix} = \begin{bmatrix} \mathsf{A} & \mathsf{B} \\ \mathsf{C} & \mathsf{D} \end{bmatrix} \begin{bmatrix} \boldsymbol{r}_1 \\ \boldsymbol{\gamma}_1 \end{bmatrix} = \mathsf{S} \begin{bmatrix} \boldsymbol{r}_1 \\ \boldsymbol{\gamma}_1 \end{bmatrix} \tag{3.1.99}$$

with the matrices A, B, C, D, and S given by comparison with the more detailed representations. Identities between the matrices, characteristic for the symplectic geometry (see Sect. 3.1.6.2.6), are: $\mathsf{A}\,\mathsf{D}^{\mathsf{T}} - \mathsf{B}\,\mathsf{C}^{\mathsf{T}} = \mathsf{I}$; $\mathsf{A}\,\mathsf{B}^{\mathsf{T}} = \mathsf{B}\,\mathsf{A}^{\mathsf{T}}$; $\mathsf{C}\,\mathsf{D}^{\mathsf{T}} = \mathsf{D}\,\mathsf{C}^{\mathsf{T}}$, and $\det \begin{vmatrix} \mathsf{A} & \mathsf{B} \\ \mathsf{C} & \mathsf{D} \end{vmatrix} = \frac{n'}{n}$, where T means the

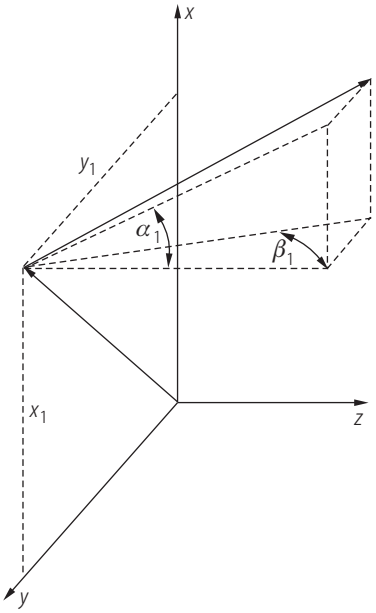

Fig. 3.1.35. Three-dimensional ray in the input plane I.

transposition of the matrix and I the identity matrix [86Sie, 05Hod]. The matrix S contains at most 10 independent parameters [76Arn, 86Sie, 05Hod].

In Table 3.1.15 general ray-transfer matrices are given.

3.1.6.2.5 General astigmatic system

A general astigmatic system can be generated by two cylindrical lenses with their axes non-parallel and non-orthogonal, separated by a distance L: $\mathsf{S}_{\mathrm{GA}} = \mathsf{R}^{-1}\,\mathsf{S}_{\mathrm{cyl},1}\,\mathsf{R}\,\mathsf{S}_{\mathrm{L}}\,\mathsf{S}_{\mathrm{cyl},2}$.

3.1.6.2.6 Symplectic optical system

Symplectic optical systems in the paraxial range can be described by the formalism of the symplectic geometry [03Wal]. They can be generated by a finite number of cylindrical and spherical lenses separated by free spaces. The mathematical formulation is connected with the matrix properties given in Sect. 3.1.6.2.4. For theoretical foundation and practical calculations see [64Lun, p. 216], [83Mac, 85Sud, 86Sie, 99Gao, 05Gro1, 05Hod].

3.1.6.2.7 Misalignments

The geometric optical calculations of *misalignments* with matrix techniques require, generally, higher dimensional matrices [05Gro1, p. 51], for example 3×3-matrices [86Sie] or 4×4-matrices [85Wan] for two-dimensional problems or 6×6-matrices for three-dimensional problems [76Arn].

Table 3.1.15. General ray-transfer matrices [99Gao, 05Hod].

Effect of the matrix	Matrix
Free propagation, index n_0, length z	$\mathsf{S}_{\mathrm{L}} = \begin{bmatrix} 1 & 0 & \frac{z}{n_0} & 0 \\ 0 & 1 & 0 & \frac{z}{n_0} \\ 0 & 0 & 1 & 0 \\ 0 & 0 & 0 & 0 \end{bmatrix}$
Aligned spherical thin lens, focal length f	$\mathsf{S}_{\mathrm{sph}} = \begin{bmatrix} 1 & 0 & 0 & 0 \\ 0 & 1 & 0 & 0 \\ \frac{-1}{f} & 0 & 1 & 0 \\ 0 & \frac{-1}{f} & 0 & 1 \end{bmatrix}$
Aligned cylindrical thin lens	$\mathsf{S}_{\mathrm{cyl}} = \begin{bmatrix} 1 & 0 & 0 & 0 \\ 0 & 1 & 0 & 0 \\ \frac{-1}{f_x} & 0 & 1 & 0 \\ 0 & 0 & 0 & 1 \end{bmatrix}$
Cylindrical telescope, m and n are the magnifications along x- and y-axis, respectively	$\mathsf{S}_{\mathrm{M}} = \begin{bmatrix} m & 0 & 0 & 0 \\ 0 & n & 0 & 0 \\ 0 & 0 & m^{-1} & 0 \\ 0 & 0 & 0 & n^{-1} \end{bmatrix}$
Rotation of the x-y-plane by the angle θ: given a system matrix S, then the rotated system matrix $\mathsf{S}_{\mathrm{rot}} = \mathsf{R}^{-1}(\theta)\,\mathsf{S}(\theta = 0)\,\mathsf{R}(\theta)$ with $\mathsf{R}^{-1}(\theta) = \mathsf{R}(-\theta) = \mathsf{R}^{\mathsf{T}}(\theta)$	$\mathsf{R} = \begin{bmatrix} \cos\theta & \sin\theta & 0 & 0 \\ -\sin\theta & \cos\theta & 0 & 0 \\ 0 & 0 & \cos\theta & \sin\theta \\ 0 & 0 & -\sin\theta & \cos\theta \end{bmatrix}$

3.1.6.3 Lens aberrations

Corrections beyond the paraxial range are required by large object-space aperture light sources like *semiconductor lasers* (large vertical far-field angles) or large image-space aperture laser focusing optics like *CD-optics*.

Shape factor of a lens:

$$q = \frac{r_2 + r_1}{r_2 - r_1}\,. \tag{3.1.100}$$

Shape factor and spherical aberration for focusing of light:

– *Minimum of spherical aberration*:

$$\frac{r_1}{r_2} = \frac{n(2n-1) - 4}{n(2n+1)}\,.$$

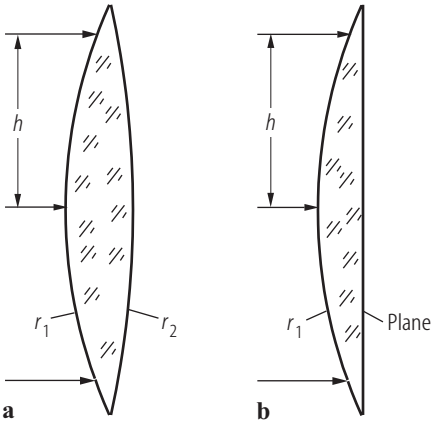

Fig. 3.1.36. Focusing of incident collimated light by (**a**) a general lens with curvature radii r_1 and r_2, (**b**) a plano-convex lens with shape factor $q = 1$.

– Refractive index $n = 1.5 \Rightarrow \dfrac{r_1}{r_2} = -\dfrac{1}{6} \Rightarrow q = 0.7\,.$

– $\left|\dfrac{r_1}{r_2}\right| \Rightarrow \dfrac{1}{\infty} \Rightarrow q = 1$ (plano-convex lens), spherical aberration near to minimum.

In Fig. 3.1.36 the focusing of incident collimated light by (**a**) a general lens with curvature radii r_1 and r_2 and (**b**) a plano-convex lens with shape factor $q = 1$ is shown.

In Table 3.1.16 the third-order spherical aberration and coma for a thin plano-convex lens is given in comparison with the diffraction-limited resolution for a plane wave or Gaussian illumination.

Remark 1: Third-order formulae for finite object distance: see [88Kle, 76Jen], more general: [80Hof, 86Haf, 96Ped, 99Bor].

Remark 2: About further third-order aberrations as astigmatism, field curvature, image distortion: see [76Jen, 78Dri, 80Hof, 86Haf, 88Kle, 96Ped, 99Bor].

Remark 3: The third-order aberrations are not exactly valid for higher apertures. Example: The third-order spherical aberration deviates for $2h/f = 1/5$ by $\approx 2\,\%$ from the ray-tracing values (the limit, recommended in [74Sle] for estimations), $h/f = 3/10$: $\approx 15\,\%$ deviation [76Jen]. Therefore, the *ray tracing* should be preferred for larger deviations from the paraxial case. It is the base of modern commercial optical design programs.

Example 3.1.14. Given: a plano-convex lens after Fig. 3.1.36b with the radius of the spherical surface $r_1 = 5$ mm, $n = 1.5$, collimated light with wavelength $\lambda = 1$ µm, stop with a height $h = 1.5$ mm, and a fiber with core diameter $2\,r = 100$ µm and numerical aperture $N.A. = 0.2$. Required: a geometric-optical estimation on the hits of the core of the fiber by the rays in the paraxial focal point and in the point of least confusion (Fig. 3.1.37). From (3.1.101)–(3.1.105): $f = 10$ mm, $\Delta s'_{\mathrm{l}} = -262$ µm, $|\Delta s'_{\mathrm{t}}| = 39$ µm, $\Delta s'_{\mathrm{lc}} = -210$ µm, $|\Delta s'_{\mathrm{tc}}| = 16$ µm, $\Delta s'_{\mathrm{tb}} = 4$ µm, and $\Delta s'_{\mathrm{tg}} = 2.1$ µm. In the paraxial focal plane as well as in the plane of least confusion, the hits of the fiber core by rays are closer than 50 µm to the optical axis and the angles of the rays with the optical axis are ≤ 0.15 within the fiber aperture. Therefore, all rays are accepted by a step-index fiber. About the analog task for Gaussian beams see references in Sect. 3.1.7.5.4 and commercial optical design programs, which show in this case, that a large part of radiation is coupled in higher-order modes.

Table 3.1.16. Third-order spherical aberration and coma for a thin plano-convex lens [76Jen, p. 152], [88Kle, p. 185], [87Nau, p. 109] in comparison with the diffraction-limited resolution for a plane wave or Gaussian illumination.

Figures	Formulae
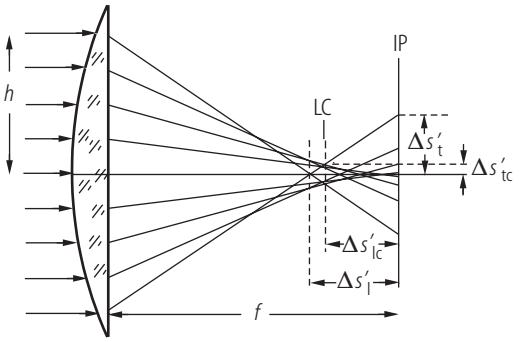 **Fig. 3.1.37.** Spherical aberration at a plano-convex lens. IP: paraxial image plane, LC: least confusion.	Lens equation (3.1.95) with $t = 0$, $a \Rightarrow -\infty$, $r_2 \Rightarrow -\infty$, $f = f'$, which is modified outside Sect. 3.1.6.1: $\frac{1}{f} = (n-1)\,\frac{1}{r_1}$, (3.1.101) $\frac{\Delta s'_l}{f} = -\frac{n^3 - 2n^2 + 2}{2n(n-1)^2}\left(\frac{h}{f}\right)^2$, (3.1.102) $\Delta s'_t = \Delta s'_l\,\frac{h}{f}$, (3.1.103) plane of least confusion [87Nau, 99Pau, 99Bor], [01Iff, p. 214]: $\Delta s'_{lc} \approx 0.8\,\Delta s'_l$, (3.1.104) $\Delta s'_{tc} \approx 0.4\,\Delta s'_t$. (3.1.105) Gaussian weights of the illumination change the geometric optical position of least confusion [01Mah].
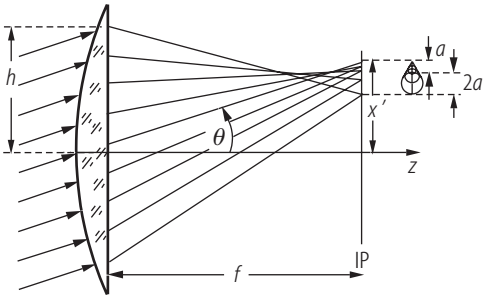 **Fig. 3.1.38.** Coma at a plano-convex lens.	$x' = \theta f$, (3.1.106) $\frac{a}{f} = -\frac{n^2 - n - 1}{2n(n-1)}\left(\frac{h}{f}\right)^2 \theta$ (3.1.107) with θ: angle of incidence.
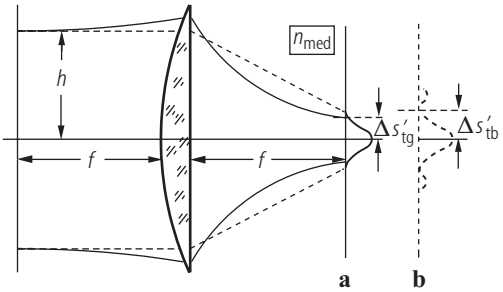 **Fig. 3.1.39.** Diffraction-limited resolution for (**a**) a Gaussian beam with waist h ($1/e^2$-intensity level) in the object-side focal plane, (**b**) a plane wave at circular stop with radius h.	$\Delta s'_{tg} = \frac{\lambda}{\pi\, n_{med}(h/f)}$, (3.1.108) $\Delta s'_{tb} = 0.61\,\frac{\lambda}{n_{med}\,\sin\sigma'} \approx 0.61\,\frac{\lambda}{n_{med}\,(h/f)}$ (3.1.109) with λ: wavelength [m], h: zonal height [m], f: focal length [m], n_{med}: refractive index of the image space.

3.1.7 Beam propagation in optical systems

Paraxial propagation of light in a system given by its ABCD-matrix can be calculated

- for (*coherent*) *Gaussian beams* by q-parameter propagation (Sect. 3.1.7.2),
- for *general field distributions* by Collins integral (Sect. 3.1.7.4),
- for *second-order moments of the electric field* by propagation of the Wigner distribution in Chap. 2.2 (beam characterization).

3.1.7.1 Beam classification

In Table 3.1.17 various types of beams are listed.

3.1.7.2 Gaussian beam: complex q-parameter and its ABCD-transformation

3.1.7.2.1 Stigmatic and simple astigmatic beams

3.1.7.2.1.1 Fundamental Mode

- *Stigmatic beam* and rotational-symmetric system:
  ⇒ both longitudinal cross sections are treated equally,
- *Simple astigmatic beam* and elements with a symmetry plane:
  ⇒ two different sets of ABCD-matrices for the tangential and sagittal cut (see Table 3.1.12).

The *introduction* of the *complex q-parameter* [66Kog1, 66Kog2]

$$\frac{1}{q_x(z)} = \frac{1}{R_x(z)} - \frac{\mathrm{i}\,\lambda}{\pi\, w_x(z)^2} \tag{3.1.110}$$

formalizes the x-part of the fundamental-mode equation (3.1.31)

$$U_0(x,z) = \sqrt{\frac{w_{0x}}{w_x(z)}}\exp\left\{-\frac{x^2}{w_x(z)^2} - \mathrm{i}\,\frac{kx^2}{2R_x(z)}\right\} \tag{3.1.111}$$

to the simple complex shape

$$U_0(x,z) = \frac{1}{\sqrt{1+\mathrm{i}\,\frac{z}{z_0}}}\exp\left\{-\mathrm{i}\,\frac{kx^2}{q_x(z)}\right\}\ . \tag{3.1.112}$$

In Fig. 3.1.40 the transfer of a field distribution by an optical system given by its ABCD-matrix is shown. In Table 3.1.18 the q-parameter transfer for stigmatic and simple astigmatic beams is given.

Table 3.1.17. Types of beams.

Beam [69Arn, 05Hod]	Generated by	Beam type is characterized by the shape of the matrix S (3.1.99)	Examples	References with practical example calculations
Stigmatic 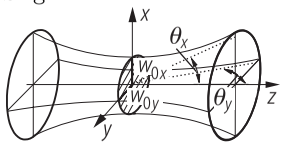	Fundamental-mode laser	$A_{xx} = A_{yy}$; $A_{xy} = A_{yx} = 0$, and the same for B, C, D	TE00-mode handling in laser applications	[75Ger, 86Sie, 91Sal], [96Yar, 01Iff, 05Hod], see Sect. 3.1.7.2.1
Simple astigmatic 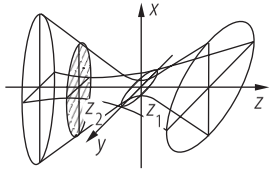	Semiconductor lasers or: Anamorphic optical system (f.e. cylindrical lens) in combination with a stigmatic beam	$A_{xx} \neq A_{yy}$; $A_{yx} = A_{xy} = 0$ (no mixing of both orthogonal planes), and the analog for B, C, D	– ring lasers, – lasers, including dispersive elements (dye-lasers), – tolerance calculations for resonators and beam-guiding optics	[05Hod, 99Gao, 86Sie], see Sect. 3.1.7.2.1
General astigmatic	General rotation of an anamorphic optics in relation with a simple astigmatic beam	General case	Transformation of higher-order radiation modes	[05Hod, 99Gao], see Sect. 3.1.7.2.2

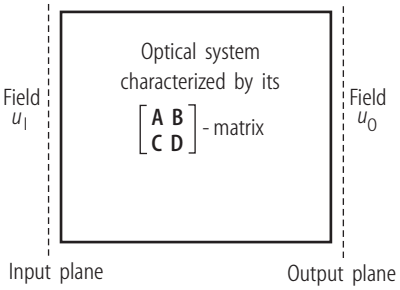

Fig. 3.1.40. Transfer of a field distribution by an optical system given by its ABCD-matrix.

Table 3.1.18. q-parameter transfer for stigmatic and simple astigmatic beams.

Given	Propagated field
– Gaussian beam in the *input* plane: $u_{\mathrm{I}}(x,z) = \exp\left\{-\mathrm{i}\,\frac{kx^2}{2q_{\mathrm{I}x}}\right\}$. (3.1.113) – ABCD-matrix of the optical system (see Tables 3.1.11 and 3.1.12). – Starting point: $R_{\mathrm{I}} = 1/\mathrm{Re}\,(1/q_{\mathrm{I}})$, $w_{\mathrm{I}} = 1/\sqrt{-\pi\,\mathrm{Im}\,(1/q_{\mathrm{I}})/\lambda}$.	– Transformation of the q-parameter: $q_{\mathrm{O}x} = \frac{Aq_{\mathrm{I}x}+B}{Cq_{\mathrm{I}x}+D}$. (3.1.114) – Field in the output plane: $u_{\mathrm{O}}(x,z) = \exp\left\{-\mathrm{i}\,\frac{kx^2}{2q_{\mathrm{O}x}}\right\}$ (3.1.115) with the real parameters of the *output* beam [96Gro]: – beam radius: $w_{\mathrm{O}x} = w_{\mathrm{I}x}\sqrt{\left(\frac{\lambda B}{\pi w_{\mathrm{I}x}^2}\right)^2 + \left(A+\frac{B}{R_{\mathrm{I}x}}\right)^2}$, (3.1.116) – curvature radius of the wavefront: $R_{\mathrm{O}x} = \frac{\left(A+\frac{B}{R_{\mathrm{I}x}}\right)^2 + \left(\frac{\lambda B}{\pi w_{\mathrm{I}x}^2}\right)^2}{\left(A+\frac{B}{R_{\mathrm{I}x}}\right)\left(C+\frac{D}{R_{\mathrm{I}x}}\right) + D\left(\frac{\lambda B}{\pi w_{\mathrm{I}x}^2}\right)^2}$. (3.1.117)

Example 3.1.15. Given: the waist of a Gaussian beam

$$u_{\mathrm{I}} = \exp\left\{-\frac{x^2}{w_0^2}\right\} = \exp\left\{-\mathrm{i}\,\frac{kx^2}{2q_1}\right\}$$

with $q_1 = \mathrm{i}\,z_0$ in comparison with (3.1.110).

Asked: free-space propagation along the distance z with the ABCD-matrix $\begin{bmatrix}1 & z\\ 0 & 1\end{bmatrix}$.

Solution:

$$q_2 = \frac{Aq_1+B}{Cq_1+D} = z + \mathrm{i}\,z_0$$

and

$$U_{\mathrm{O}} = \left(A+\frac{B}{q_1}\right)^{-1/2}\exp\left\{-\mathrm{i}\,\frac{kx^2}{2q_2}\right\} = \left(1+\frac{z}{\mathrm{i}\,z_0}\right)^{-1/2}\exp\left\{-\mathrm{i}\,\frac{kx^2}{2(z+\mathrm{i}\,z_0)}\right\} .$$

3.1.7.2.1.2 Higher-order Hermite-Gaussian beams in simple astigmatic beams

Treatment of the x- or y-component of Hermite-Gaussian-beams after (3.1.27): The complex q-parameter transformation is treated as above, the fundamental mode part is given as above, the new beam radius for the Hermite polynom of order m, $H_m(\sqrt{2}\,x/w_{\mathrm{I}x})$ is calculated from the new q-parameter and the phase is derived from it, too [70Col].

For complex Hermite-Gaussian beams: see [86Sie].

3.1.7.2.2 General astigmatic beam

In Table 3.1.19 the Q^{-1}-matrix transfer for general astigmatic beams is given. The matrix Q^{-1} is the matrix scheme of inverses of q-parameters and no inverted matrix [96Gro].

Table 3.1.19. Q^{-1}-matrix transfer for general astigmatic beams.

Given	Propagated field
– General Gaussian beam in the input plane: $$U_{\mathrm{I}}(\boldsymbol{r}) = \exp\left\{-\mathrm{i}\,\frac{k}{2}\,\boldsymbol{r}\,\mathsf{Q}_{\mathrm{I}}^{-1}\,\boldsymbol{r}\right\}\,, \quad (3.1.118)$$ $\boldsymbol{r} \sim (x, y)$ the transverse position vector perpendicular to the propagation axis z. – $\mathsf{Q}_{\mathrm{I}}^{-1}$-matrix: $$\mathsf{Q}_{\mathrm{I}}^{-1} = \begin{bmatrix} \frac{1}{q_{xx}} & \frac{1}{q_{xy}} \\ \frac{1}{q_{xy}} & \frac{1}{q_{yy}} \end{bmatrix} \quad (3.1.119)$$ with q_{xx}, q_{xy}, q_{yy} complex terms describing the general amplitude- and phase-distribution of U_{I}, and $$\boldsymbol{r}\,\mathsf{Q}_{\mathrm{I}}^{-1}\,\boldsymbol{r} = \frac{x^2}{q_{xx}} + 2\frac{xy}{q_{xy}} + \frac{y^2}{q_{yy}}\,. \quad (3.1.120)$$ – S-matrix of the optical system (see Table 3.1.15) with $$\mathsf{S} = \begin{bmatrix} \mathsf{A} & \mathsf{B} \\ \mathsf{C} & \mathsf{D} \end{bmatrix}$$ after (3.1.99).	– Transformation of the $\mathsf{Q}_{\mathrm{I}}^{-1}$-matrix to its output value: $$\mathsf{Q}_{\mathrm{O}}^{-1} = \left(\mathsf{C} + \mathsf{D}\,\mathsf{Q}_{\mathrm{I}}^{-1}\right)\left(\mathsf{A} + \mathsf{B}\,\mathsf{Q}_{\mathrm{I}}^{-1}\right)^{-1}\,, \quad (3.1.121)$$ see [88Sim, 96Gro, 05Hod]. – Field in the output plane: $$U_{\mathrm{O}}(\boldsymbol{r}) = \exp\left\{-\mathrm{i}\,\frac{k}{2}\,\boldsymbol{r}\,\mathsf{Q}_{\mathrm{O}}^{-1}\,\boldsymbol{r}\right\}\,. \quad (3.1.122)$$

Example 3.1.16. Transformation of a simple astigmatic Gaussian beam (no mixing between x and y) with a θ-rotated cylindrical lens to a general astigmatic beam: We start with $\mathsf{Q}_{\mathrm{I}}^{-1} = \begin{bmatrix} \frac{1}{q_{xx}} & 0 \\ 0 & \frac{1}{q_{yy}} \end{bmatrix}$. The rotation of an x-aligned cylindrical lens, given as $\mathsf{S}_{\mathrm{cyl}}$ in Table 3.1.15, is performed by multiplying first $\mathsf{S}_{\mathrm{cyl}}$ with the rotation matrix R of Table 3.1.15, and then the product with the inverse of R is:

$$\mathsf{S}_{\text{rotated cyl.}} = \mathsf{R}^{-1}\,\mathsf{S}_{\text{cyl}}\,\mathsf{R} = \begin{bmatrix} \mathsf{A} & \mathsf{B} \\ \mathsf{C} & \mathsf{D} \end{bmatrix}$$

with

$$\mathsf{A} = \begin{bmatrix} 1 & 0 \\ 0 & 1 \end{bmatrix}, \quad \mathsf{B} = \begin{bmatrix} 0 & 0 \\ 0 & 0 \end{bmatrix}, \quad \mathsf{C} = \begin{bmatrix} -\cos^2\theta/f_x & -\sin\theta\,\cos\theta/f_x \\ -\sin\theta\,\cos\theta/f_x & -\sin^2\theta/f_x \end{bmatrix}, \quad \mathsf{D} = \begin{bmatrix} 1 & 0 \\ 0 & 1 \end{bmatrix}$$

and

$$\mathsf{Q}_{\mathrm{O}}^{-1} = \begin{bmatrix} -\cos^2\theta/f_x + 1/q_{xx} & -\sin\theta\,\cos\theta/f_x \\ -\sin\theta\,\cos\theta/f_x & -\sin^2\theta/f_x + 1/q_{yy} \end{bmatrix}.$$

Therefore, the output field

$$u_{\mathrm{O}}(\boldsymbol{r}) = \exp\left\{-\mathrm{i}\,\frac{k}{2}\left[\left(-\frac{\cos^2\theta}{f_x} + \frac{1}{q_{xx}}\right)x^2 - 2\,\frac{\sin\theta\,\cos\theta}{f_x}xy + \left(-\frac{\sin^2\theta}{f_x} + \frac{1}{q_{yy}}\right)y^2\right]\right\}$$

is a general astigmatic Gaussian beam with a mixing term between the coordinates x and y.

3.1.7.3 Waist transformation

Often, the transfer of the beam waist is required for instance for focusing of laser light. Then, the following algorithms are *much more simple* than the q-parameter algorithm.

3.1.7.3.1 General system (fundamental mode)

In Table 3.1.20 the waist transformation for a general system is given.

3.1.7.3.2 Thin lens (fundamental mode)

The formulae (3.1.123)–(3.1.126) are further simplified using the focal length f for the thin lens only, see Table 3.1.21.

Remark: Discussion of equation (3.1.127):

The right-hand-side term of (3.1.127) containing z_0 represents the *modification* introduced by the Gaussian beam optics to the thin-lens equation ((3.1.95), $t \Rightarrow 0$) shown in Fig. 3.1.42.

In Fig. 3.1.43 the relation of the Gaussian waist transfer to the thin-lens equation of geometrical optics for different influences of diffraction is shown.

Main modifications of the geometrical optics:

- No "image distance" is at infinity.
- For $z = f$ (point P) the image is at $z' = f$ (transfer of the object-side focal plane to the image-side focal plane after (3.1.130), not $\Rightarrow \infty$).
- If a target z'-position is given, then two starting z-positions are possible.

Example 3.1.17. Given for Fig. 3.1.42: $z = 1179$ mm, $w_0 = 0.22$ mm, $\lambda = 1.06$ µm; it follows $z' = 109$ mm, $w_0' = 0.02$ mm, $\theta' = 0.96°$, and $z_0' = 1.21$ mm. The second right-hand term of (3.1.127) translates the Gaussian waist image by 0.16 mm in comparison with the geometrical optical image towards the lens.

Table 3.1.20. Waist transformation for a general system.

Given	Solution
– ABCD-matrix of the system, – waist w_0, – wavelength λ, including $z_0 = \pi w_0^2/\lambda$, – distance z to the input plane of the system.	$z' = \begin{cases} \dfrac{-(Az+B)(Cz+D) - ACz_0^2}{C^2 z_0^2 + (Cz+D)^2} & \text{for } C \neq 0\,, \\ -\dfrac{Az+B}{D} & \text{for } C = 0\,, \end{cases}$ (3.1.123)
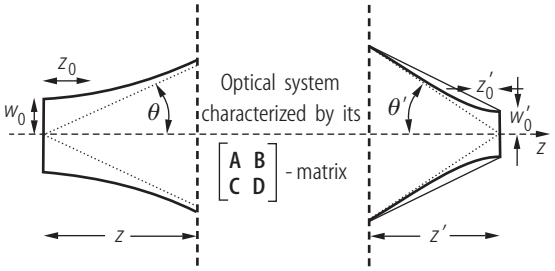	$z_0' = z_0 \left[\dfrac{Cz'+A}{Cz+D}\right] = \dfrac{z_0}{C^2 z_0^2 + (Cz+D)^2}$, (3.1.124)
Fig. 3.1.41. Waist transformation by an optical system.	$w_0' = \sqrt{\dfrac{\lambda z_0'}{\pi}}$, (3.1.125)
Asked: Waist w_0' and distance z' to the output plane of the system including z_0'.	$\Theta_0' = \sqrt{\dfrac{\lambda}{\pi z_0'}}$. (3.1.126)
	The *beam parameter product* is invariant: $w_0' \Theta_0' = w_0 \Theta_0 = \lambda/\pi$.

Table 3.1.21. Waist transformation by a thin lens.

Given	Solution
– Focal length f of the lens, – wavelength λ, – waist w_0, including $z_0 = \pi w_0^2/\lambda$, – distance z to the input plane of the system.	$\dfrac{1}{z} + \dfrac{1}{z'} = \dfrac{1}{f} + \dfrac{z_0^2}{z\,[z^2 + z_0^2 - zf]}$, (3.1.127)
	see Fig. 3.1.42,
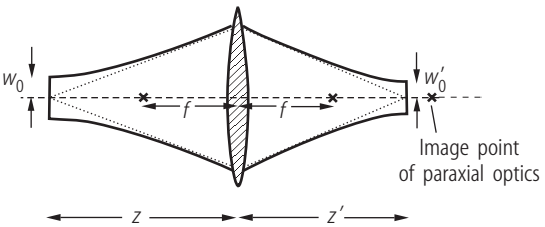	$w_0' = w_0 \dfrac{f}{\sqrt{z_0^2 + (z-f)^2}}$, (3.1.128)
	$z_0' = \dfrac{\pi w_0'^2}{\lambda}$. (3.1.129)
Fig. 3.1.42. Waist transformation by a thin lens.	If $z = f$, then
Asked: Waist w_0' and distance z' to the output plane of the system and z_0'.	$z' = f$ and $w_0' = \dfrac{w_0 f}{z_0}$. (3.1.130)

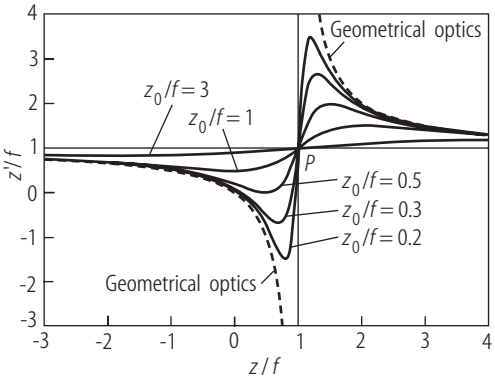

Fig. 3.1.43. Relation of the Gaussian waist transfer (full lines) to the thin-lens equation (dashed) of geometrical optics for different influences of diffraction (wavelength λ respectively z_0).

3.1.7.4 Collins integral

For Fresnel's approximation of diffraction in paraxial systems see [68Goo, 71Col, 78Loh, 94Roe]. It was generalized to the propagation of field distributions in ABCD-described systems by [70Col, 76Arn, 05Gro2, 05Hod].

3.1.7.4.1 Two-dimensional propagation

In Table 3.1.22 the propagation in rotational symmetric systems and simple astigmatic systems is given.

Table 3.1.22. Propagation in rotational symmetric systems and simple astigmatic systems.

Given	Solution
– ABCD-matrix of the optical system (see Tables 3.1.11 and 3.1.12), – field distribution in the input plane $U_\mathrm{I}(x)$, – path length along the optical axis L.	Field $U_\mathrm{O}(x_2)$ in the output plane (*Collins integral*): $U_\mathrm{O}(x_2) = \sqrt{\frac{\mathrm{i}}{\lambda B}}\ \mathrm{e}^{-\mathrm{i}kL}$ $\times \int_{-\infty}^{\infty} \mathrm{d}\,x_1\, U_\mathrm{I}(x_1) \exp\left\{-\mathrm{i}\,\frac{k}{2B}\left[Ax_1^2 - 2x_1x_2 + Dx_2^2\right]\right\}.$ (3.1.131)

Example 3.1.18. The waist of a Gaussian beam is given with $U_\mathrm{I}(x_1) = \exp\left(-x_1^2/w_\mathrm{I}^2\right)$ in the input plane. The system consists of a thin lens with the focal length f followed by a free-space propagation by distance z. The ABCD-matrix is calculated from Fig. 3.1.34 and Table 3.1.11:

$$\begin{bmatrix} A & B \\ C & D \end{bmatrix} = \begin{bmatrix} 1 - z/f & z \\ -1/f & 1 \end{bmatrix}.$$

$$U_\mathrm{O}(x_2) = \sqrt{\frac{\mathrm{i}}{\lambda z}}\ \mathrm{e}^{-\mathrm{i}kL} \int_{-\infty}^{\infty} \mathrm{d}\,x_1 \exp\left(-\frac{x_1^2}{w_\mathrm{I}^2}\right) \exp\left\{-\mathrm{i}\,\frac{k}{2z}\left[\left(1 - \frac{z}{f}\right)x_1^2 - 2x_1x_2 + x_2^2\right]\right\}.$$

The result is an output Gaussian intensity distribution with the waist radius

$$w_{\mathrm{O}} = \frac{w_{\mathrm{I}}}{\sqrt{1 + \left(\frac{\pi w_{\mathrm{I}}^2}{\lambda f}\right)^2}} ,$$

the waist position $z = z_{\mathrm{waist}} = f \left(\frac{\pi w_{\mathrm{O}} w_{\mathrm{I}}}{\lambda f}\right)^2$, and $z_{\mathrm{O}} = \pi w_{\mathrm{O}}^2/\lambda$.

For inclusion of *displacements and misalignments* in Collins Integral see [96Tov].

3.1.7.4.2 Three-dimensional propagation

In Table 3.1.23 the propagation in in general astigmatic systems is given.

Table 3.1.23. Propagation in general astigmatic systems.

Given	Solution
– S: matrix of the optical system, see Table 3.1.15 and (3.1.99) with $\mathsf{S} = \begin{bmatrix} \mathsf{A} & \mathsf{B} \\ \mathsf{C} & \mathsf{D} \end{bmatrix}$,	Field $U_{\mathrm{O}}(\boldsymbol{r}_2)$ in the output plane (*Collins integral*): $U_{\mathrm{O}}(\boldsymbol{r}_2) = \frac{-\mathrm{i}\exp(-\mathrm{i}kL)}{\lambda\sqrt{\det \mathsf{B}}} \int\int \mathrm{d}\,\boldsymbol{r}_1 U_{\mathrm{I}}(\boldsymbol{r}_1)$ $\times \exp\left\{-\mathrm{i}\frac{k}{2}\left[\boldsymbol{r}_1 \mathsf{B}^{-1} \mathsf{A}\,\boldsymbol{r}_1 - 2\,\boldsymbol{r}_1 \mathsf{B}^{-1}\,\boldsymbol{r}_2 + \boldsymbol{r}_2 \mathsf{D}\,\mathsf{B}^{-1}\,\boldsymbol{r}_2\right]\right\}$ (3.1.132)
– field distribution in the input plane: $U_{\mathrm{I}}(\boldsymbol{r}_1)$, where $\boldsymbol{r}_1$ is the position vector in the input plane.	with $\det \mathsf{B}$ the determinant and B^{-1} the inverse of the matrix B. Examples in [70Col, 05Gro2, 05Hod].

3.1.7.5 Gaussian beams in optical systems with stops, aberrations, and waveguide coupling

3.1.7.5.1 Field distributions in the waist region of Gaussian beams including stops and wave aberrations by optical system

Classical cases of *optical system design* are given in [99Bor, 80Hof, 86Haf]. [82Wag, 95Gae] use the calculation of the field distribution in the image by a stop and wave aberrations in the exit pupil.

The analog is modeled for Gaussian beams on the exit pupil in the following references:

- focused Gaussian beams with aberrations and stops: see [69Cam, 71Sch],
- obscuration of a rotationally symmetrical Gaussian beam including longitudinal focal shift: see [82Car, 86Sta],
- extended systematic discussion of diffraction with stops, obscuration, and aberrations: see [86Mah, 01Mah],
- spherical aberration: see [98Pu].

3.1.7.5.2 Mode matching for beam coupling into waveguides

The calculation of the excitation coefficient of an eigenmode in a waveguide (output mode) by the incident mode (input mode) at the surface of the waveguide is described in Table 3.1.24.

This task occurs

- if a laser beam is formed by an optical system and coupled afterwards into an optical fiber,
- if a laser beam of a master oscillator is to be coupled into a power amplifier,
- in the case of waveguide-waveguide coupling especially fiber-fiber coupling or coupling between semiconductor lasers.

Solutions are available in commercial optical design programs.

Table 3.1.24. Definitions for waveguide coupling.

Given	Solution
– Incident beam (emitted by a laser (and) transformed by an optical system): $E_{\text{input}}(x, y)$. – Waveguide with an eigenmode field the coupling to which is asked: $E_{\text{output}}(x, y)$. 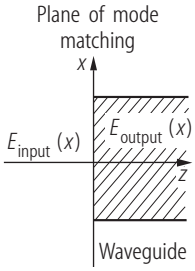 **Fig. 3.1.44.** Mode matching. *Asked:* Part of power transmitted into the waveguide (fiber, laser, integrated optical waveguide).	*Coupling coefficient* (power relation): $\eta = \dfrac{O_{\text{IO}}\, O^*_{\text{IO}}}{N_{\text{I}}\, N_{\text{O}}}$. (3.1.133) *Overlap integral*: $O_{\text{IO}} = \int\limits_{-\infty}^{\infty} \mathrm{d}\,x \int\limits_{-\infty}^{\infty} \mathrm{d}\,y\, E_{\text{I}}(x, y)\, E^*_{\text{O}}(x, y)$. (3.1.134) *Normalization*: $N_{\text{I}} = \int\limits_{-\infty}^{\infty} \mathrm{d}\,x \int\limits_{-\infty}^{\infty} \mathrm{d}\,y\, E_{\text{I}}(x, y)\, E^*_{\text{I}}(x, y)$. (3.1.135) *Normalization*: $N_{\text{O}} = \int\limits_{-\infty}^{\infty} \mathrm{d}\,x \int\limits_{-\infty}^{\infty} \mathrm{d}\,y\, E_{\text{O}}(x, y)\, E^*_{\text{O}}(x, y)$. (3.1.136) Effective antireflection layers are assumed to be on the waveguide.

3.1.7.5.3 Free-space coupling of Gaussian modes

For the case that a Gaussian output waist of a source waveguide and a Gaussian input waist of a receiver waveguide are separated by air, the coupling of both waveguides is generally treated in [64Kog]. Higher-order modes are also included. The approximation of small misalignments (offset and tilt) is given in Table 3.1.25, large offsets and tilts are treated in [64Kog, 91Wu].

Table 3.1.25. Coupling of waveguides .

Given	Solution
– Source WG1 (laser, waveguide) which emits a Hermite-Gaussian beam, – receiver WG2 (laser, waveguide) which can accept Hermite-Gaussian eigenmodes: 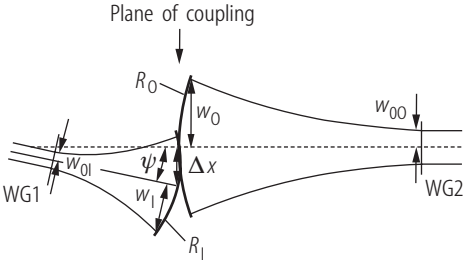 **Fig. 3.1.45.** Coupling of Gaussian beams. $w_{0\,\mathrm{I}}$ and $w_{0\,\mathrm{O}}$: beam waist radii for WG1 and WG2, respectively; w_I and w_O: beam radii in the coupling plane; R_I and R_O: curvature radii of the beam wavefronts in the coupling plane; $k = 2\pi/\lambda$; λ: the wavelength of light; Δx: the lateral offset between the waveguides; ψ: the tilt of the axis. *Asked*: The efficiency of the excitation of the modes in WG2, here the fundamental mode 00.	$$\eta_{00-00} = \frac{4}{\left(\frac{w_\mathrm{I}}{w_\mathrm{O}} + \frac{w_\mathrm{O}}{w_\mathrm{I}}\right)^2 + \left(\frac{\pi\, w_\mathrm{I}\, w_\mathrm{O}}{\lambda}\right)^2 \left(\frac{1}{R_\mathrm{I}} - \frac{1}{R_\mathrm{O}}\right)^2} - \frac{8\,(w_{0\,\mathrm{I}}\, w_{0\,\mathrm{O}}\, \Delta x)^2}{\left(w_{0\,\mathrm{I}}^2 + w_{0\,\mathrm{O}}^2\right)^3} - \frac{k^2\,\psi^2}{2}\left(w_\mathrm{I}^2 + w_\mathrm{O}^2\right) .$$ (3.1.137) $\eta_{00-00} = 1$ for $\Delta x = \psi = 0$ and the exact beam radii and curvature fitting $w_\mathrm{I} = w_\mathrm{O}$ and $R_\mathrm{I} = R_\mathrm{O}$, otherwise $\eta_{00-00} < 1$. Equation (3.1.137) contains the approximations: – Gaussian beams (paraxial optics). – Right-hand side of (3.1.137): 2nd and 3rd term $\ll$ 1st term. About coupling coefficients for higher-order modes and without the approximation: see [64Kog]; on couplings with Hermite-Gaussian modes and Laguerre-Gaussian modes: see [94Kri, 80Gra].

3.1.7.5.4 Laser fiber coupling

Methods of treatment:

– Launching of *fundamental-mode laser radiation* into the *fundamental mode* of a single-mode fiber:
  – Calculation of the overlap integral (3.1.134) for a Gaussian mode and the mode field for different fiber cross sections: see [88Neu, p. 179], [80Gra].
  – Approximation of the exact fiber fundamental modes by a Gaussian field distribution (see [88Neu, pp. 68]) and the application of the waist transformation from laser via an optical system with the methods of Sects. 3.1.7.2–3.1.7.4 and calculation of the overlap integral equation (3.1.134) or mode-coupling equation (3.1.137) [91Wu].

– Launching of fundamental-mode laser radiation or *multimode laser radiation* or incoherent light sources into *multimode fibers*:
  – Overlap integral techniques in the framework of partial coherence theory: see [87Hil].
  – Geometric optical methods (ray tracing and phase space techniques): see [90Gec, 95Sny, 91Gra, 91Wu, 01Iff].

– Inclusion of the *aberrations and stops* of the optical system used:
  – Monomodal and partial coherent case: calculation of the wave aberrations of the optical system by ray-tracing methods and inclusion of these aberrations into the overlap integral: see [82Wag, 95Gae, 89Hil, 99Gue].
  – Ray-tracing methods are adequate for stops and aberrations, but not reliable for a few mode waveguides: rough design [01Iff]: the spot diagram of the ray tracing in the fiber facet should be within the core area and the angles of incidence should be smaller then the aperture angle [88Neu] of the fiber.